Available online at www.sciencedirect.com
SCIENCE DIRECT®
Organic Geochemistry 37 (2006) 408–427
Organic Geochemistry
www.elsevier.com/locate/orggeochem

# Reactive polar precipitation via ether cross-linkage: A new mechanism for solid bitumen formation

Clifford C. Walters [a,*], Simon R. Kelemen [a], Peter J. Kwiatek [a], Robert J. Pottorf [b], Paul J. Mankiewicz [b], David J. Curry [c], Kevin Putney [d]

[a] *ExxonMobil Research and Engineering Co., Corporate Strategic Research, 1545 Route 22 East, Annandale, NJ 08801-0998, United States*
[b] *ExxonMobil Upstream Research Co., 2189 Buffalo Speedway, Houston, TX 77252-2189, United States*
[c] *ExxonMobil Exploration Co., 233 Benmar, Houston, TX 77060-2501, United States*
[d] *ExxonMobil Development Co., 12450 Greenspoint Drive, Houston, TX 77060-1905, United States*

Received 7 October 2005; received in revised form 6 December 2005; accepted 7 December 2005
Available online 20 February 2006

**Abstract**

Analysis of solid bitumens from the Tengiz Field, Kazakhstan by X-ray photoelectron spectroscopy provides evidence for a new reservoir alteration process – reactive polar precipitation via the formation of ether cross-linkages. Solid bitumens, which may occupy >30% of the pore space, were analyzed in situ and as isolated concentrates of the material in vein/fracture-fills or encapsulated within micropores. Their compositions were found to vary greatly, particularly in the amounts of aromatic carbon and in the organic oxygen mostly present in C–O single bond environments. While most solid bitumen in Tengiz reservoir rocks arose from asphaltene precipitates, surfaces are coated with a relatively aliphatic- and oxygen-rich material. Organic sulfur occurs exclusively in aromatic sulfur environments in most samples, while nitrogen is in pyrrolic and pyridinic environments. To account for the average organic composition of solid bitumen, we propose that the coatings are formed by condensation of low-molecular weight polar compounds that are normally soluble in most oils. A likely reaction mechanism involves free radicals, produced by thermally labile non-aromatic sulfur (–SH) forms, reacting with hydroxyls. This reaction results in a release of $H_2S$ and the formation of compounds with at least one ether-linkage and multiple heteroatoms within the aromatic cores. Similar reactions are believed to convert the reactive polar precipitate and previously precipitated asphaltenes into toluene-insoluble bitumens. This hypothesis explains the chemical nature of the solid bitumens, accounts for previously reported anomalies in reflectance, and is fully consistent with current geohistory models. Whether this reservoir alteration process occurs outside of the North Caspian Basin is not known, but we suspect that the process occurs elsewhere. Thin coatings of polar precipitates, which may be undetectable by conventional optical microscopy, could have significant impact on reservoir properties, such as surface wetability or mineral diagenesis.


## 1. Introduction

Solid bitumens are viscous or solid petroleum residues that fill reservoir pore space (Rogers et al., 1974). These organic materials may dissolve in laboratory solvents, but are insoluble at subsur-

* Corresponding author. Tel.: +1 908 730 3166; fax: +1 908 730 3031.
*E-mail address:* clifford.c.walters@exxonmobil.com (C.C. Walters).

0146-6380/$ - see front matter © 2005 Elsevier Ltd. All rights reserved.
doi:10.1016/j.orggeochem.2005.12.007

face conditions and resist reservoir remediation efforts. Solid bitumens have been described in oil fields worldwide and their presence can have detrimental effects on production (Lomando, 1992). Solid bitumens reduce porosity and permeability of reservoir rocks by filling or lining pore spaces and by restricting and closing pore throats. Their occurrence can cause significant reservoir heterogeneity and wetability inversions that negate effective response to stimulation practices (Patel et al., 1987). Although solid bitumen behaves as cement, neutron logs record this immobile organic matter as porosity and resistivity logs record it as conventional oil pay, complicating estimates of recoverable reserves.

Solid bitumens can form from a variety of processes (Curiale, 1986; Peters et al., 2004). Pyrobitumens are highly aromatic residues that form via thermal cracking of hydrocarbons ( $\gtrsim 170$ °C) or by oxidative processes associated with thermochemical sulfate reduction ( $\gtrsim 140$ °C). Solid bitumens also may arise from several low-temperature processes. Severe biodegradation can alter oil to form viscous tars that may not flow under reservoir conditions. Asphaltenes may precipitate from crude oils by the addition of light hydrocarbons or by depressurization of the reservoir. These low-temperature organic solids may be further altered by sulfur-incorporation (vulcanization) or by subsequent thermal annealing.

The bulk of the Tengiz reservoir organic solids clearly arose from precipitated asphaltenes, though the manner of their alteration from asphaltenes to solid residues remains in question (Warner et al., 1999; Pottorf et al., 2003). We present evidence for a novel mechanism for the formation of thin coatings of solid bitumens that exist on surfaces of Tengiz reservoir rocks and asphaltic solid bitumen cores via the precipitation of low molecular-weight polar compounds after the formation of ether cross-linkages under reservoir conditions (<120 °C). These reactions produce organic solids on organic or mineral surfaces that are chemically distinct from asphaltene precipitates and pyrobitumens. Such reactions appear to be responsible for the conversion of precipitated asphaltenes into insoluble residues.

### 1.1. Geologic setting

Samples used in this study are from well cores from the Tengiz Field, North Caspian Basin, Kazakhstan – a supergiant field with ~6–9 billion bbl of estimated recoverable oil reserves (Effimoff, 2001). Tengiz is one of several isolated carbonate buildups with Devonian – Carboniferous reservoirs in the larger Primorskoye uplift. Tengiz Field comprises a relatively flat platform interior, a structural high that rims the platform, and a flank facies that developed downslope of the platform (Lisovsky et al., 1992). This carbonate buildup resembles modern day constructional carbonate platforms, such as the Caribbean Andros Island platform, in size and shape. North Caspian buildups are distinct in they typically have several kilometers of prograding Serpukhovian (lower Carboniferous) platform facies that contain microbial boundstones and associated debris-flow facies (James et al., 2003; Weber et al., 2004).

Three reservoir units are defined in Tengiz that correspond to a sequence stratigraphic framework (Harris et al., 2000; James et al., 2003; Weber et al., 2004) (Fig. 1). The lowermost, Unit 3, is a broad Late Devonian carbonate platform. Unit 2, the middle ~600 m of the reservoir, represents punctuated backsteps during the Tournaisian and Viséan stages. Carbonate deposition was interrupted by volcanics during the mid-Viséan time; and, when resumed, formed Unit 1, the upper ~450 m of reservoir. This unit is characterized by platform progradation during the Serpukhovian, with growth terminated by platform drowning during the Early Bashkirian. The structure is overlain by a thin layer of Artinskian shale and a thick layer of Kungurian evaporites that provide effective seals.

Hydrocarbons are produced mainly from the Unit 1 platform carbonates, which consists of cyclic deposits of grainstones and packstones that sometimes are capped by thin, low-porosity beds (Harris et al., 2001; James et al., 2003). The cycles are <5 m thick in the Bashkirian (top-most ~100 m) and up to 30 m thick in the Serpukhovian and Late Viséan intervals. Porosity can be highly variable within each cycle and includes inter-particle, vuggy, moldic, and some fracture porosity. In the platform rim and flanks, microbial boundstones form thick reservoir rocks consisting of either in-place upper slope or transported lower-slope debris deposits (Harris and Warner, 2001; James et al., 2003; Weber et al., 2004). Unit 2 consists of grainstones and packstones that have local porosity, but diminish in reservoir quality with depth. Unit 3 consists of Devonian carbonates that underlie the central platform.

Organic-rich facies of the Devonian Domanik Formation and basinal Carboniferous carbonates

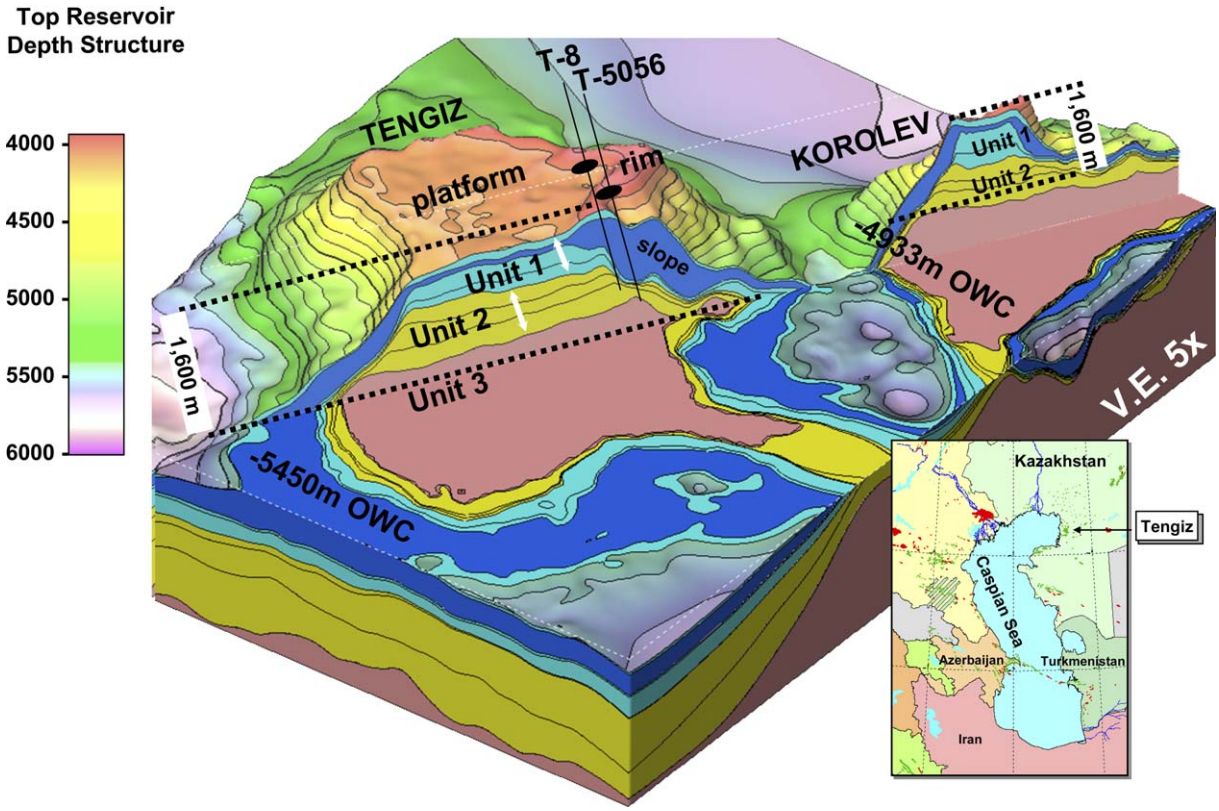


Fig. 1. The structure of Tengiz and Korolev Fields is illustrated in 3D-perspective by a depth map to the top of the Carboniferous Bashkarian. Tengiz consists of a relatively flat platform interior, a topographic high that rims the platform, and the flanks that consist mostly of debris slope deposits. The field is defined by three production units which are illustrated in the cut through of the platform. Locations and depth penetrations of the T-8 and T-5056 wells, which provided the solid bitumen samples used in this study, are shown.

are considered to be the main source rocks for hydrocarbons in Tengiz (Lisovsky et al., 1992; Schoellkopf and Hallager, 1998). The paragenetic sequence of carbonate deposition, dissolution, bitumen formation, sparry calcite cementation, and late dolomitization indicates a complex geohistory of hydrocarbon entrapment and leakage and mineral diagenesis. Several geohistory models have been proposed that attempt to account for these observations (Hallager et al., 1997; Schoellkopf and Hallager, 1998; Warner et al., 1999; Anissimov et al., 2000). The current consensus is that Tengiz was charged initially with asphaltene-bearing oil ~200–165 Ma ago. Seal failure from ~165 to 125 Ma resulted in depressurization of the reservoir with brines re-saturating most of the stratigraphic units. Re-establishment of the seal at ~125 Ma allowed for a second hydrocarbon charge and a latter addition of $H_2S$ generated by thermochemical sulfate reduction of basinal, offstructure hydrocarbons.

### 1.2. Solid bitumens at Tengiz Field

Solid bitumen is common throughout Tengiz Field, though its abundance varies with stratigraphy and location, and is most abundant in the shallowest Bashkirian and Serpukhovian reservoir intervals and in the platform rim where it may occupy >30% of the available porosity. Solid bitumen occurs as coatings on carbonate grains, as linings in micropores, and as void fills within large pores (Hwang et al., 1998). A close relationship between fractures and elevated bitumen levels is observed, particularly in thin sections from wells penetrating elevated platform rim and flank facies (Pottorf et al., 2003).

Tengiz solid bitumen originated from secondary organic matter that was once mobile. Bitumen in macropores may exhibit meniscus-like surfaces and display medium to coarse-grained microtexture with anisotropic character indicating that they are derived from an asphaltene-rich precursor (Tver-

dova et al., 1991; Hwang et al., 1998). Fluid inclusion analysis indicates that some asphaltene precipitation resulted from reservoir depressurization (Tseng and Pottorf, 2003). Alternatively, asphaltene precipitation could have resulted from the mixing of incompatible petroleum fluids and gases. Both processes concentrated asphaltene precipitates in areas of enhanced fluid flow, which accounts for the common occurrence of fractures filled with solid bitumen. Microbial boundstones that formed in Tengiz rim and flank facies are prone to fracturing, facilitating the vertical migration of hydrocarbons. Multiple pore volumes of hydrocarbons are thought to have moved through areas of Tengiz along major migration pathways at times of peak hydrocarbon migration. This increases the risk of porosity occlusion by solid bitumens along these pathways. In contrast with the Tengiz margin, the platform interior has a smaller volume of solid bitumen that tends to concentrate near the base of depositional cycles, possibly due to gravitational settling of asphaltenes. Asphaltenes converted to solid bitumens via thermal alteration under elevated, hydrothermal (Karpov et al., 1985; Schoellkopf and Hallager, 1998; Warner et al., 1999) or normal reservoir temperatures (Pottorf et al., 2003; Tseng and Pottorf, 2003). We propose that, in addition to thermal alteration, an alternative mechanism is partially responsible for converting asphaltenes to solid bitumens at Tengiz and for precipitating reactive polar compounds that form naphthenic-rich solid residues.

## 2. Experimental

### 2.1. Solid bitumen samples and sample preparation

Solid bitumens analyzed in this study are from core samples taken from the T-8 and T-5056 wells located along the northern portion of the Tengiz platform rim (Fig. 1). Samples from the T-8 are restricted to Bashkirian (Late Mississippian) to Late Viséan (Early Pennsylvanian) Unit 1 reservoir. Samples from the T-5056 well include this range and extend into older early Viséan to Tournaisian (Middle to Early Mississippian) Unit 2 and Famennian (Late Devonian) Unit 3 reservoirs (Fig. 2). These wells are in are the rim facies of the field where solid bitumens are particularly abundant, typically filling 10–20% of the pore space.

Two types of solid bitumens were separated from these samples. Macroscopic solid bitumens filling fractures or coating carbonate minerals could be analyzed in situ, or as easily isolated, homogenized solids removed from the rock. The second type of solid bitumen fills micropores and appears to be totally encapsulated by the carbonate matrix. We developed three sample preparations to provide samples suitable for analysis by X-ray photoelectron spectroscopy (XPS). These are designated in the text as ''small spot'', ''vein-fill'', or ''encapsulated''. We avoided the use of strong acids, which are used routinely to dissolve carbonate minerals, in order to eliminate potential chemical alteration of the bitumen. Care was taken in all procedures to minimize air exposure to avoid surface oxidation.

#### 2.1.1. Small spot (110 μm/slot)

For the small-spot analysis, freshly chipped portions of core (~1–2 mm in diameter) were prepared, revealing fresh surfaces of solid bitumen that occur primarily in fractures and vein-fills. These samples were mounted directly on a sample holder and placed into the vacuum chamber without further preparation. Surfaces were then scanned optically for solid bitumen particles ~500 μm or more in diameter that were deemed suitable areas for collecting data. A 110 μm spot size or a slot analysis (an ellipsoidal ~400 μm region) was used as the analyzer acceptance area depending on the required spatial resolution. Analyses of several individual solid bitumen occurrences from within the same sample are possible.

#### 2.1.2. Vein-fill

Core samples were lightly fractured into small grains using vise-grips with approximately 1 mm opening. The process dislodged many of the carbonaceous flecks that were usually associated with fractures. The flecks were placed within a small vial filled with toluene that, when agitated, resulted in a suspension of small (<10 μm) carbonaceous and inorganic particles. Following agitation and settling of the larger carbonate particles after few seconds, toluene with the suspended fines was drawn off with a bulb pipette and transferred to a small mortar. The solvent was allowed to evaporate from the mortar and the residue was ground, producing a homogenized composite of solid bitumen from larger veins and fracture surfaces. These samples were sufficiently enriched to obtain high-quality XPS data from the carbonaceous material, composed mostly of insoluble solid bitumen with only trace amounts of solubilized hydrocarbons.

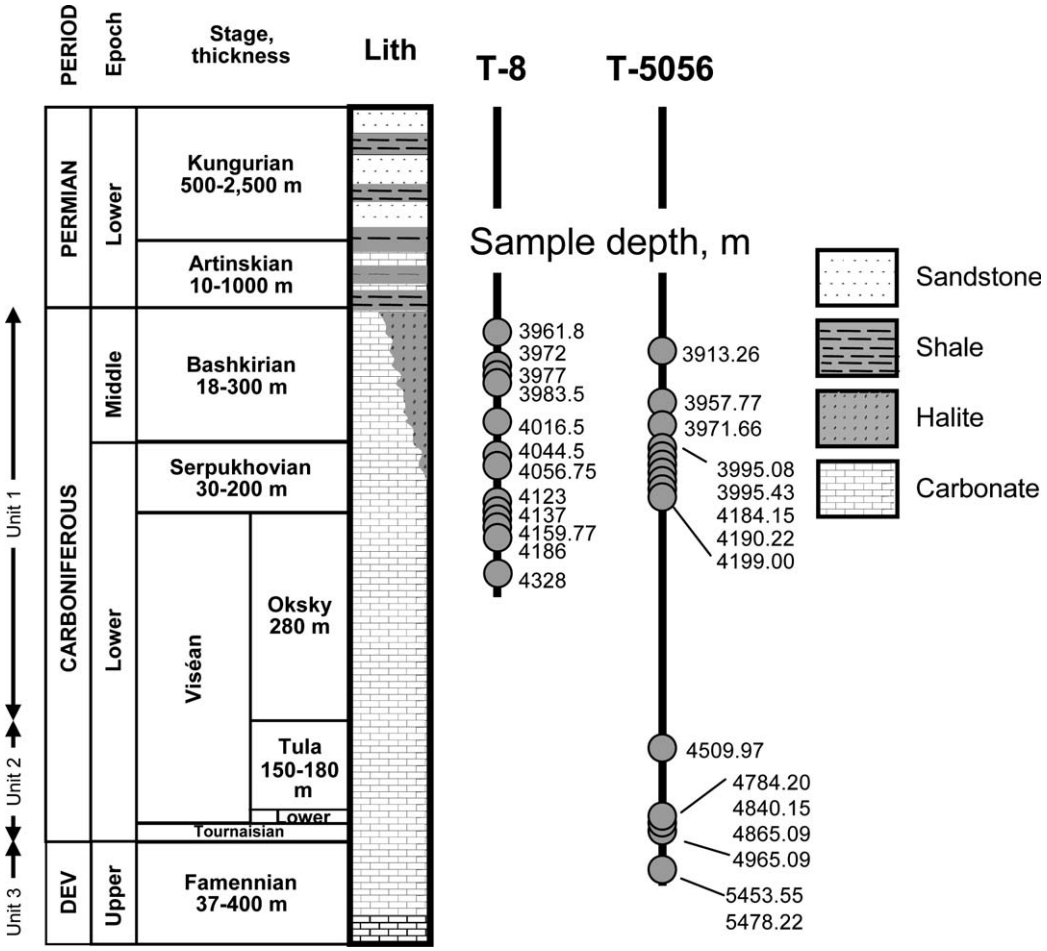


Fig. 2. Stratigraphic column and solid bitumen sample depths from the T-8 and T-5056 wells.

*2.1.3. Encapsulated*

To recover and enrich bitumen from micropores, a carbonate core sample was lightly crushed and sorted by size. Grains that appeared to have solid bitumen encapsulated within the calcite matrix from the >100 mesh (~74 μm) to <200 (~149 μm) mesh sieve fraction were selected manually with tweezers. These grains were then finely ground (<3 μm) using a Wig-L-bug™ grinding apparatus to expose the solid bitumen, producing a light gray calcite-solid bitumen powder. Samples were analyzed with no additional treatment.

*2.2. X-ray photoelectron spectroscopy (XPS)*

XPS analyses were conducted using a Kratos Axis Ultra system equipped with a monochromatic Al Kα radiation source and automatic charge neutralization (Fig. 3). Solid bitumen samples were mounted on a metallic sample nub using Scotch double-sided non-conducting tape. An energy correction was made to account for sample charging based on the carbon (1s) peak at 285.0 eV. Survey spectra were obtained at a pass energy of 160 eV with a step size of 500 meV. Survey spectra are suitable to determine total elemental composition, but generally do not allow sufficient resolution to determine chemical speciation and/or oxidation state of individual elements. High-resolution spectra were obtained for selected elements using an analyzer pass energy of 40 eV and an energy step size of 100 meV. Under these conditions the full width at half maximum of a paraffin wax standard sample was ~1.1 eV. These spectra can be curve-resolved into a series of peaks, each of which represents a different chemical environment. The element's oxidation state and the nature of its bonds with other elements influence the energy position of each peak. The curve resolved peaks can be

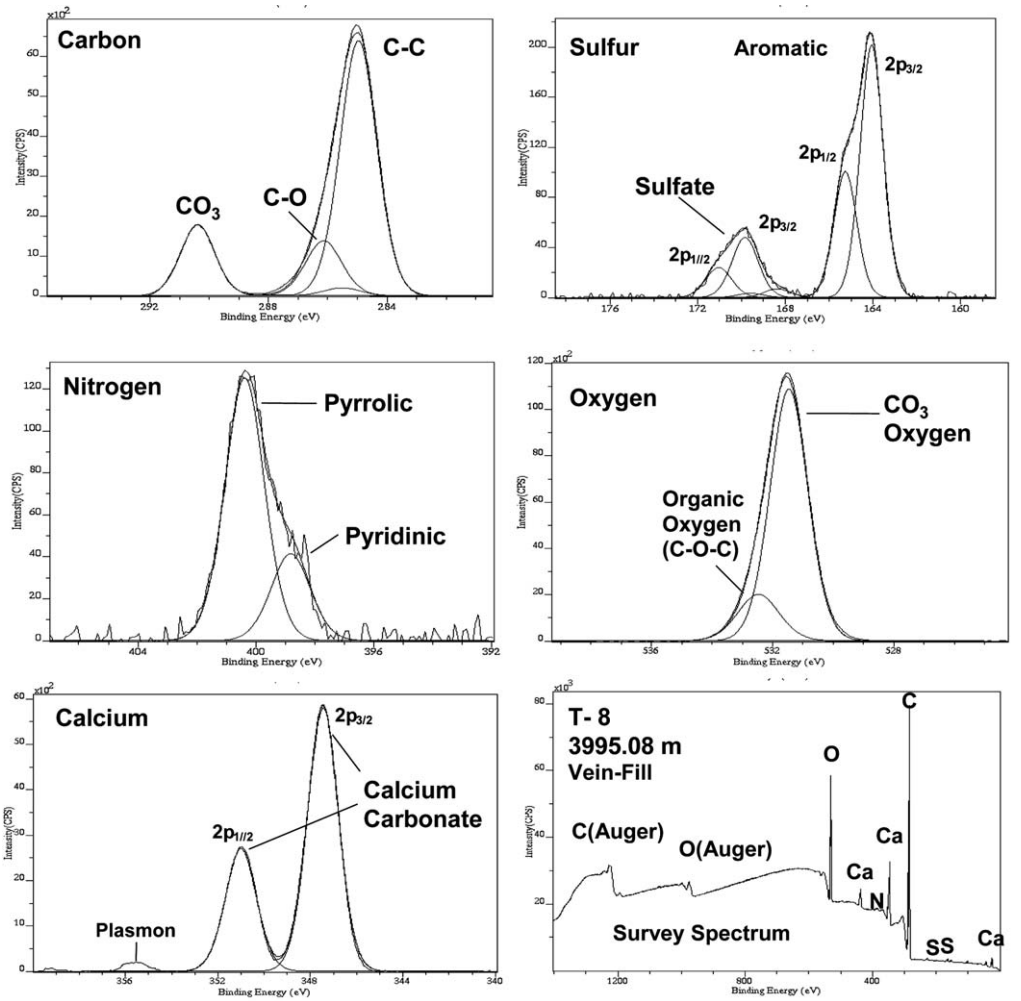


Fig. 3. C, S, N, O, and Ca high-resolution survey XPS spectra for a representative vein-fill sample.

related to specific chemical speciations based on comparisons of the chemical energy shifts with standard compounds and materials.

Resolution of the carbon (1s) spectra followed the method of (Kelemen and Kwiatek, 1995). Five chemical environments of organic carbon are identified: (1) aromatic and aliphatic carbon, (2) carbon bound to oxygen by a single bond (i.e., ethers and hydroxyls), (3) carbon bound to oxygen by two bonds (i.e., carbonyl), (4) carbon bound to oxygen by three bonds (i.e., carboxyl), and (5) beta carbon defined as carbon adjacent to carboxyl carbon or carbon bound to nitrogen (i.e., pyrrolic or pyridinic). Carbonate carbon appears as a distinct peak at 290.5 eV. The relative amount of aromatic carbon was determined by following the method of Kelemen et al. (1993) from the calibrated intensity of the $\pi \rightarrow \pi^*$ signal intensity.

Resolution of the nitrogen (1s) spectra followed the method of Kelemen et al. (1994, 1999, 2002). Two chemical environments are identified: (1) pyridinic nitrogen, and (2) pyrrolic nitrogen. Resolution of the sulfur (2p) spectra followed the method of Kelemen et al. (1990). Four chemical environments are found at energy positions consistent with: (1) non-aromatic (i.e., sulfidic) sulfur, (2) aromatic sulfur (i.e., thiophenic, arylsulfide), (3) sulfite ($SO_3$), and (4) sulfate ($SO_4$).

Each oxygen (1s) spectrum was curve-resolved using three peaks at 531.5 eV (inorganic oxygen), 532.5 eV (organic oxygen) and 533.5 eV (organic oxygen) having a mixed Gaussian–Lorentzian line shape and a peak width at half-maximum of 1.6 ($\pm$0.2) eV for each peak. The dominance of carbonate oxygen in some samples prevents quantitative curve resolution of other components. In samples

with minimal carbonate interference, organic oxygen spectra were consistent with the carbon (1s) spectra and indicate that carbon–oxygen single-bond species are the only chemical environment found for organic oxygen in almost all Tengiz samples. Each calcium (2p) spectrum was curve-resolved into $2p_{3/2}$ and $2p_{1/2}$ components. All calcium XPS spectra are consistent with calcium carbonate.

A complete discussion of XPS precision and reproducibility is beyond the scope of this paper, but is covered in the references listed above. The large disparity in some values between samples that appear to be duplicates (i.e., same well/same depth) is real as these samples represent different spatially resolved analyses from the same core sample. As such, they are as unique from each other as are samples from different depths and wells.

## 3. XPS results

### 3.1. Survey spectral analysis

Elemental data from a rapid survey scan are listed in Tables 1a and 1b for samples from the T-8 and T-5056 wells, respectively. The spectra obtained from the Tengiz samples are typically mixtures of solid bitumen and calcite, with minor amounts of trace minerals such as anhydrite, dolomite, clays, and halite.

### 3.2. High-resolution spectral analysis

High-resolution spectra were obtained for carbon on all samples and on other elements for selected samples (Tables 2a and 2b). The organic carbon is mostly associated with aliphatic and aromatic hydrocarbon bonds. Few or no carbonyl or carboxyl groups are present, but a significant number of C–O bonds (e.g., ethers and furans) are revealed. Beta carbon is not well defined in encapsulated samples and is included with the main 1s carbon. Organic sulfur was found to be bound exclusively as aromatic sulfur (i.e., thiophenic, arylsufides) for nearly all samples. The proportion of organic sulfur to sulfate was highly variable with sulfate accounting for up to 98% of the observed sulfur. This is true not only for ground samples where anhydrite was included, but also

Table 1a
Elemental survey scans

| Depth (m) | Prep/anal. | N | O | S | Si | Al | Ca | Mg | Na | Cl |
|---|---|---|---|---|---|---|---|---|---|---|
| 3961.8 | Vein-fill | **1.0** | **21.2** | **0.7** | 0.8 | 0 | **5.6** | 0 | 0 | 0 |
| 3961.8 | Slot | 0.4 | **80.2** | **1.7** | 0 | 0 | **22.4** | 0 | 1.1 | 0.2 |
| 3961.8 | Encapsulated | **1.1** | **78.9** | **1.3** | 0.5 | 0 | **23.0** | 0 | 0 | 0.6 |
| 3961.8 | Encapsulated | **1.1** | **59.3** | **1.7** | 0 | 0 | **17.6** | 0 | 0 | 0 |
| 3972 | Vein-fill | **0.9** | **35.8** | **1.8** | 0.2 | 0 | **0** | 0 | 0 | 0 |
| 3972 | Slot | 0.8 | **24.9** | **1.1** | 0.6 | 0 | **3.8** | 0.3 | 0.4 | 0 |
| 3972 | Encapsulated | **1.1** | **66.4** | **1.9** | 0 | 0 | **19.6** | 0 | 0 | 0.3 |
| 3977 | Vein-fill | **0.5** | **40.0** | **1.5** | 0.4 | 0 | **11.4** | 0.1 | 0 | 0 |
| 3977 | Slot | **1.0** | **67.4** | **2.4** | 0.4 | 0 | **17.9** | 0.7 | 0.7 | 0 |
| 3983.5 | Slot | **5.0** | **48.2** | **2.1** | 0 | 0 | **12.5** | 0.2 | 0.5 | 0 |
| 3983.5 | Slot | **0.4** | **65.3** | **1.9** | 0.2 | 0 | **18.3** | 0 | 1 | 0 |
| 3983.5 | Encapsulated | **0.6** | **73.3** | **1.8** | 0 | 0 | **21.4** | 0 | 0 | 0.4 |
| 4016.5 | Slot | **3.3** | **23.6** | **0.5** | 1.4 | 0 | **1.6** | 0.4 | 0.1 | 0 |
| 4016.5 | Encapsulated | **0.4** | **93.5** | **1.3** | 0.3 | 0 | **28.2** | 0 | 0 | 0.6 |
| 4044.5 | Slot | 0.6 | **23.5** | **0.8** | 1.2 | 0 | **0** | 0 | 0.4 | 0 |
| 4044.5 | Slot | **0.3** | **18.8** | **1.1** | 0.4 | 0 | **1.7** | 1.2 | 0.2 | 3.6 |
| 4044.5 | Encapsulated | **0.5** | **86.0** | **1.3** | 0 | 0 | **17.8** | 9.3 | 0 | 0.5 |
| 4056.75 | Encapsulated | **0.8** | **65.3** | **1.6** | 0 | 0 | **19.4** | 0 | 0 | 0.4 |
| 4056.75 | Slot | 1.4 | **22.4** | **1.8** | 0.7 | 0 | **9.5** | 0.2 | 0.2 | 0 |
| 4123 | Slot | **1.6** | **66.6** | **1.8** | 0.7 | 0.2 | **0** | 0.2 | 1.1 | 0 |
| 4123 | Encapsulated | **0.4** | **70.1** | **1.4** | 0 | 0 | **20.1** | 0.6 | 0 | 0.4 |
| 4137 | Slot | **1.1** | **53.4** | **1.3** | 0.7 | 0 | **13.0** | 0.8 | 0.6 | 0 |
| 4157.77 | Slot | 1.4 | **24.9** | **1.3** | 0.1 | 0 | **7.0** | 0 | 0 | 0 |
| 4186 | Vein-fill | **0.5** | **37.0** | **1.1** | 0.3 | 0 | **10.4** | 0.4 | 0.1 | 0 |
| 4186 | Slot | **1.2** | **50.7** | **1.6** | 0.4 | 0 | **12.6** | 1.1 | 0 | 0 |
| 4328 | Vein-fill | **0.4** | **17.8** | **0.6** | 0.5 | 0 | **5.0** | 0 | 0 | 0 |
| 4328 | Slot | **1.1** | **39.5** | **1.0** | 0.6 | 0 | **10.9** | 0.2 | 0.4 | 0 |

T-8 well samples atoms per 100 carbon atoms.

Table 1b
Elemental survey scans

| Depth (m) | Prep/anal. | N | O | S | Si | Al | Ca | Mg | Na | Cl |
|---|---|---|---|---|---|---|---|---|---|---|
| 3913.26 | Vein-fill | **1.4** | **30.9** | **1.6** | 0.3 | 0 | **8.9** | 0 | 0 | 0.3 |
| 3913.26 | Slot | **2.9** | 3.8 | **2.3** | 0.5 | 0 | 10.1 | 0 | 0 | 0 |
| 3957.77 | 110 μm | 1.8 | 66.4 | 1.1 | 0.2 | 0 | 0 | 0 | 0.5 | 0 |
| 3957.77 | Slot | **2.5** | 76.4 | **1.4** | 0 | 0 | 24.2 | 0 | 0.6 | 0.3 |
| 3995.08 | 110 μm | 0.7 | 43.3 | 0.8 | 1.4 | 0 | 9 | 0 | 0 | 0.1 |
| 3995.08 | 110 μm | 1.6 | 41.0 | 1.2 | 2.0 | 0 | 5.5 | 0 | 0 | 0 |
| 3995.08 | 110 μm | 0.4 | 0 | 0.8 | 0 | 0 | 8.5 | 0 | 0 | 0 |
| 3995.08 | 110 μm | 0.1 | 0 | 0.6 | 0 | 0 | 6.3 | 0 | 0 | 0 |
| 3995.08 | 110 μm | 1.0 | 0 | 0.8 | 0.0 | 0 | 4.9 | 0 | 0 | 0 |
| 3995.08 | Vein-fill | **1.5** | **45.5** | **1.7** | 0.6 | 0 | **12.9** | 0 | 0 | 0 |
| 3995.43 | 110 μm | 2.2 | 57.5 | 0.8 | 1.4 | 0.7 | 0 | 0 | 0.6 | 0 |
| 3995.43 | Vein-fill | **0.2** | **68.3** | **0.6** | 0.3 | 0 | **19.8** | 0 | 0.4 | 0.3 |
| 3995.43 | Slot | **2.4** | 67.4 | **1.3** | 0.4 | 0 | 19.6 | 0.5 | 0 | 0 |
| 4190.22 | Slot | 1.0 | 66.9 | 0.7 | 0.6 | 0 | 16.0 | 0.3 | 0.5 | 0 |
| 4199.85 | Encapsulated | 1.3 | 120.7 | 1.3 | 0.4 | 0 | 37.0 | 0.3 | 0.3 | 0 |
| 4199.85 | 110 μm | 0.8 | 55.7 | 0.5 | 0.9 | 0 | 13.2 | 0 | 0.4 | 0 |
| 4199.85 | 110 μm | 2.1 | 59.2 | 0.7 | 0.4 | 0 | 15.0 | 0 | 0.2 | 0 |
| 4199.85 | 110 μm | 0.7 | 77 | 0.7 | 0.0 | 0 | 22.2 | 0 | 0.6 | 0 |
| 4199.85 | Vein-fill | **0.9** | **51.7** | **1.0** | 0.6 | 0 | **14.8** | 0 | 0 | 0.8 |
| 4199.85 | Encapsulated | 0.5 | 100.7 | 1.2 | 0 | 0 | 32.0 | 0.2 | 0 | 0 |
| 4509.97 | 110 μm | 1.8 | 40.5 | 1.1 | 0.9 | 0.4 | 6.8 | 0 | 0 | 0 |
| 4509.97 | 110 μm | 1.2 | 25.5 | 0.8 | 0.0 | 0 | 1.7 | 0 | 0 | 0 |
| 4509.97 | 110 μm | 0.4 | 31.7 | 0.3 | 0.4 | 0 | 5.7 | 0 | 0 | 0 |
| 4509.97 | 110 μm | 1.3 | 27.5 | 0.5 | 1.1 | 0 | 1.3 | 0 | 0 | 0 |
| 4509.97 | Vein-fill | **0.8** | **62.3** | **0.7** | 0.4 | 0 | **18.6** | 0 | 0 | 0.3 |
| 4509.97 | Encapsulated | 2.2 | 347.8 | 5.8 | 0.6 | 0 | 108 | 1 | 2.2 | 0 |
| 4509.97 | Encapsulated | 0.5 | 118.2 | 1.8 | 0.2 | 0 | 37.3 | 0.2 | 0 | 0 |
| 4784.26 | 110 μm | 0.3 | 128.8 | 0.8 | 1.0 | 0 | 35.4 | 0 | 0 | 0 |
| 4784.26 | 110 μm | 1.1 | 129 | 0.9 | 0.0 | 0 | 54.8 | 0 | 0.7 | 0 |
| 4784.26 | Encapsulated | 0 | 2.3 | 0.2 | 0.3 | 0 | 45.7 | 1.3 | 1 | 1.4 |
| 4784.26 | Encapsulated | 0.9 | 140.1 | 1.4 | 0.8 | 0 | 43.5 | 0.5 | 0 | 0 |
| 4840.15 | Vein-fill | **1.1** | **46.5** | **0.6** | 0.6 | 0.2 | **13.6** | 0 | 0 | 0 |
| 4840.15 | Slot | 0.3 | 32.9 | **0.4** | 0.3 | 0 | 6.6 | 0.2 | 0.2 | 0 |
| 4865.09 | Encapsulated | 0.3 | 151.9 | 1.5 | 0.2 | 0 | 46.1 | 0.8 | 0.5 | 1.4 |
| 4865.09 | 110 μm | 0.0 | 185.1 | 1.6 | 0.7 | 0 | 42.1 | 0.7 | 1.1 | 0 |
| 4865.09 | 110 μm | 0.0 | 188.2 | 1.0 | 0.0 | 0 | 46.2 | 1.7 | 1.1 | 0 |
| 4865.09 | 110 μm | 0.4 | 104.9 | 0.7 | 0.0 | 1.4 | 27.8 | 0 | 0 | 0 |
| 4865.09 | 110 μm | **0.3** | 124.0 | **2.0** | 0.0 | 0 | 31.0 | 0 | 0 | 2.7 |
| 4865.09 | Encapsulated | 0.1 | 151.5 | **1.0** | 0 | 0 | 46.5 | 0.7 | 0 | 0 |
| 5433.55 | 110 μm | 0.6 | 0 | **0.4** | 0 | 0 | 23.3 | 0 | 0 | 0 |
| 5453.55 | Encapsulated | 0.3 | 142.9 | 2.3 | 0.5 | 0 | 42.3 | 1.3 | 0.8 | 0 |
| 5453.55 | Encapsulated | 0.6 | 129.1 | 1.4 | 0.5 | 0 | 40 | 0.4 | 0 | 0 |
| 5463.55 | 110 μm | 0.7 | 0 | 0.5 | 0.0 | 0 | 11.3 | 0 | 0 | 0 |
| 5478.22 | 110 μm | 1.1 | 81.6 | 1.2 | 0.0 | 0 | 24.6 | 0 | 0 | 0 |
| 5478.22 | 110 μm | **1.0** | 59.9 | **0.5** | 0.9 | 0 | 17.2 | 0 | 0 | 0 |
| 5478.22 | Vein-fill | **1.2** | **59.2** | **0.5** | 0.7 | 0 | **17.1** | 0 | 0 | 0 |
| 5478.22 | Encapsulated | 0.3 | 120.9 | **1.0** | 0.2 | 0 | 38 | 0.4 | 0 | 1.1 |

T-5056 well samples atoms per 100 carbon atoms.
Fe, K, and F, 0 for all samples; slot or 110 μm, spatially resolved solid bitumen within whole rock sample; vein-fill, solid bitumen concentrate after toluene extraction/density separation; encapsulated, ground calcite-encapsulated solid bitumen.
Survey scans in bold indicate that a high-resolution analyses was performed for this element along with carbon.

for small spot analyses where solid bitumen surfaces were targeted. Only organic nitrogen was detected. Pyrrolic nitrogen accounts for ~80% (ranging from 69% to 95%) with the balance being pyridinic. Most of the observed oxygen is resolved as inorganic and is associated with the calcium as calcite. XPS carbon (1s) curve resolution results indicate that the organic oxygen, quantified by oxygen (1s) curve resolution results, is dominated by carbon–oxygen single-bond species.

Table 2a
T-8 well samples – high-resolution elemental analyses

| Depth (m) | Prep/anal. | Per 100 carbon atoms | | | | | | | Sulfur | | | | | Nitrogen | | | Oxygen | | | | CalciumPer 100 C |
|---|---|---|---|---|---|---|---|---|---|---|---|---|---|---|---|---|---|---|---|---|---|
| | | %Aro | Main | Beta | C–O | C=O | O–C=O | $CO_3$ | Per 100 C | Mole % | | | | Per 100 C | Mole% | | Per 100 C | Mole% | | | |
| | | | | | | | | | | Non-aromatic | Aromatic | $SO_3$ | $SO_4$ | | Pyridinic | Pyrrolic | | O-inorg | O-Org1 | O-Org2 | |
| 3961.8 | Vein-fill | 28 | 86.6 | 1.7 | 5.8 | 0.1 | 0 | 5.8 | 0.8 | 0 | 75 | 16 | 9 | 0.8 | 8 | 92 | 22.6 | 85 | 14 | 1 | 5.5 |
| 3961.8 | Slot | 51 | 58.9 | 2.7 | 9.7 | 0.1 | 0 | 28.5 | 2.2 | 0 | 45 | 0 | 55 | | | | 153 | 91 | 8 | 1 | 39.6 |
| 3961.8 | Encapsulated | 59 | 57.1 | 0 | 9.1 | 0 | 0 | 33.7 | 1.5 | 0 | 92 | 0 | 8 | 0.9 | 25 | 75 | 139 | 93 | 6 | 1 | 39.6 |
| 3961.8 | Encapsulated | 58 | 64.7 | 0 | 10.4 | 0 | 0 | 24.9 | 2.0 | 0 | 91 | 0 | 9 | 0.8 | 24 | 76 | 108 | 92 | 6 | 2 | 29.5 |
| 3972 | Vein-fill | 51 | 72 | 2 | 10.6 | 3.4 | 0 | 11.9 | 2.0 | 4 | 70 | 15 | 11 | 1.0 | 31 | 69 | 48.7 | 85 | 14 | 1 | 12.5 |
| 3972 | Slot | 20 | 79.3 | 1.9 | 10.7 | 0.9 | 0 | 7.2 | 0.6 | 0 | 54 | 0 | 45 | | | | 14.5 | 52 | 37 | 11 | 2.2 |
| 3972 | Encapsulated | 63 | 61.2 | 0 | 10.6 | 0 | 0 | 28.2 | 2.2 | 0 | 90 | 0 | 10 | 1.1 | 33 | 67 | 121 | 93 | 6 | 2 | 34.1 |
| 3977 | Vein-fill | 49 | 71.7 | 4.5 | 9 | 0.4 | 0 | 14.3 | 3.1 | 1 | 89 | 2 | 8 | 1.5 | 31 | 69 | 111 | 93 | 5 | 2 | 30.2 |
| 3977 | Slot | 68 | 69 | 2.1 | 6.5 | 0.7 | 0 | 21.7 | 2.6 | 0 | 58 | 5 | 38 | 1.2 | 29 | 71 | 70.1 | 91 | 9 | 0 | 28.2 |
| 3983.5 | Slot | 42 | 71.3 | 1.9 | 8.1 | 1.1 | 0.9 | 16.7 | 2.3 | 1 | 43 | 8 | 49 | 3.8 | 4 | 96 | 62.8 | 82 | 17 | 1 | 18.4 |
| 3983.5 | Slot | 43 | 69.6 | 0.9 | 6.2 | 0.6 | 0 | 22.7 | 3.8 | 0 | 36 | 3 | 61 | 0.7 | 30 | 70 | 96.5 | 91 | 9 | 0 | 27.9 |
| 3983.5 | Encapsulated | 58 | 59.2 | 0 | 10.5 | 0 | 0 | 30.3 | 2.0 | 0 | 91 | 0 | 9 | 0.5 | 29 | 71 | 147 | 94 | 4 | 2 | 40.7 |
| 4016.5 | Slot | 26 | 82.4 | 1.2 | 10.1 | 0.1 | 4.2 | 2 | 0.4 | 0 | 31 | 48 | 22 | 1.3 | 10 | 90 | 24.2 | 32 | 59 | 8 | 1.7 |
| 4016.5 | Encapsulated | 44 | 52.7 | 0 | 8 | 0 | 0 | 39.3 | 1.4 | 0 | 81 | 0 | 19 | 0.5 | 23 | 77 | 197 | 94 | 5 | 1 | 56.5 |
| 4044.5 | Slot | 21 | 78.7 | 1.6 | 11.7 | 0.7 | 6 | 1.2 | 0.7 | 0 | 22 | 0 | 78 | | | | 19.8 | 3 | 59 | 38 | 0.9 |
| 4044.5 | Slot | 56 | 74.1 | 6.5 | 11.6 | 0.4 | 4.8 | 2.6 | 0.9 | 0 | 64 | 11 | 25 | 0.3 | 27 | 73 | 18.3 | 38 | 39 | 23 | 1.6 |
| 4044.5 | Encapsulated | 49 | 55.4 | 0 | 8.9 | 0 | 0 | 35.6 | 1.7 | 0 | 92 | 0 | 8 | 0.5 | 29 | 71 | 172 | 94 | 5 | 0 | 30.8 |
| 4056.75 | Encapsulated | 54 | 62.8 | 0 | 10 | 0 | 0 | 27.2 | 1.8 | 0 | 96 | 0 | 4 | 0.7 | 31 | 69 | 125 | 93 | 7 | 0 | 33.6 |
| 4056.75 | Slot | 65 | 70.2 | 1.6 | 14.8 | 2.2 | 1.9 | 9.4 | 1.6 | 0 | 72 | 0 | 28 | | | | 71.3 | 83 | 13 | 5 | 15.2 |
| 4123 | Slot | 61 | 68.4 | 0.4 | 10.6 | 1.7 | 0 | 19 | 1.8 | 0 | 50 | 9 | 42 | 1.9 | 20 | 80 | 103 | 92 | 8 | 0 | 25.1 |
| 4123 | Encapsulated | 54 | 61.5 | 0 | 9.9 | 0 | 0 | 28.5 | 1.7 | 0 | 95 | 0 | 5 | 0.8 | 28 | 72 | 140 | 92 | 8 | 0 | 36.7 |
| 4137 | Slot | 72 | 53.6 | 4.8 | 16.5 | 2.2 | 0 | 23.1 | 2.3 | 0 | 54 | 16 | 30 | 1.3 | 30 | 70 | 160 | 92 | 8 | 0 | 40.6 |
| 4157.77 | Slot | 46 | 81.4 | 1.9 | 8.5 | 0.7 | 0 | 7.6 | 1.2 | 0 | 82 | 3 | 15 | | | | 40.1 | 79 | 18 | 3 | 9.4 |
| 4186 | Vein-fill | 36 | 71.8 | 2.3 | 13.7 | 0.3 | 0 | 11.9 | 1.0 | 0 | 84 | 2 | 14 | 0.4 | 22 | 78 | 44.1 | 87 | 13 | 0 | 11.6 |
| 4186 | Slot | 45 | 74.6 | 0.7 | 6.1 | 0.4 | 0 | 18.2 | 1.9 | 0 | 58 | 2 | 39 | 0.7 | 28 | 72 | 76.6 | 85 | 15 | 0 | 19.4 |
| 4328 | Vein-fill | 26 | 88 | 1.1 | 4.7 | 0 | 0 | 6.2 | 0.6 | 5 | 78 | 7 | 10 | 0.3 | 9 | 91 | 20 | 84 | 14 | 2 | 5.4 |
| 4328 | Slot | 30 | 76.1 | 1.5 | 8 | 0.4 | 0 | 14 | 0.8 | 0 | 59 | 7 | 34 | 0.4 | 9 | 91 | 47.2 | 92 | 8 | 0 | 11.9 |

Table 2b
T-5056 well samples – high-resolution elemental analyses

| Depth (m) | Prep/anal. | Per 100 carbon atoms | | | | | | | Sulfur | | | | | Nitrogen | | | Oxygen | | | | Calcium |
|---|---|---|---|---|---|---|---|---|---|---|---|---|---|---|---|---|---|---|---|---|---|
| | | %Aro | Main | Beta | C–O | C=O | O–C=O | $CO_3$ | Per 100 C | Mole% | | | | Per 100 C | Mole% | | Per 100 C | Mole% | | | Per 100 C |
| | | | | | | | | | | Non-aromatic | Aromatic | $SO_3$ | $SO_4$ | | Pyridinic | Pyrrolic | | O-inorg | O-Org1 | O-Org2 | |
| 3913.26 | Vein-fill | 17 | 75.6 | 1.4 | 11.2 | 0.5 | 0 | 11.2 | 1.7 | 0 | 84 | 0 | 16 | 1.5 | 20 | 80 | 37.6 | 87 | 11 | 2 | 11.7 |
| 3913.26 | Slot | 14 | 65.2 | 0.4 | 4.3 | 0 | 0 | 30.1 | 1.9 | 0 | 40 | 0 | 60 | 2.2 | 24 | 76 | | | | | |
| 3957.77 | 110 μm | 52 | 75.1 | 0.9 | 4.7 | 1.1 | 0 | 18.1 | 1.1 | | 44 | | 66 | | | | | | | | |
| 3957.77 | Slot | 45 | 74.5 | 0.9 | 10.9 | 0 | 0 | 13.7 | 1.9 | 0 | 47 | 2 | 51 | 2.2 | 14 | 73 | | | | | |
| 3995.08 | 110 μm | 21 | 80.1 | 2 | 8.3 | 0.7 | 0 | 8.9 | 0.8 | | 44 | | 56 | | | | | | | | |
| 3995.08 | 110 μm | 24 | 73.7 | 1.8 | 17.5 | 1.7 | 0 | 5.4 | 1.2 | | 28 | | 72 | | | | | | | | |
| 3995.08 | 110 μm | 45 | 77.1 | 4.4 | 11.6 | 0 | 0 | 7.0 | 0.8 | | 41 | | 59 | | | | | | | | |
| 3995.08 | Vein-fill | 62 | 66.2 | 2.1 | 14.3 | 0.2 | 0 | 17.2 | 1.7 | 0 | 76 | 0 | 35 | 1.3 | 25 | 75 | 58.9 | 83 | 17 | 0 | 17.4 |
| 3995.43 | 110 μm | 63 | 66.8 | 0.8 | 19.1 | 1 | 0 | 5.6 | 0.8 | | 26 | | 74 | | | | | | | | |
| 3995.43 | Vein-fill | 28 | 67.3 | 1.7 | 5.1 | 0 | 0 | 25.8 | 0.6 | 0 | 50 | 9 | 41 | 0.3 | 24 | 76 | 80 | 94 | 4 | 1 | 24.2 |
| 3995.43 | Slot | 35 | 71.0 | 0.8 | 6.8 | 0 | 0 | 21.3 | | | | | | 3.3 | 18 | 82 | | | | | |
| 4190.22 | Slot | 15 | 61.7 | 2.4 | 17.3 | 0 | 0 | 18.6 | 0.7 | | 13 | | 87 | | | | | | | | |
| 4199.5 | Encapsulated | 40 | 45.5 | 0 | 6.8 | 0 | 0 | 47.7 | 1.3 | | 13 | | 87 | | | | | | | | |
| 4199.5 | 110 μm | 38 | 74.3 | 1.4 | 7.8 | 2.6 | 0 | 14.0 | 1.9 | 0 | 100 | 0 | 0 | 1.7 | 21 | 79 | | | | | |
| 4199.85 | 110 μm | 27 | 69.5 | 0 | 15 | 0 | 0 | 15.5 | 0.5 | | 44 | | 56 | | | | | | | | |
| 4199.85 | 110 μm | 25 | 73.9 | 1.5 | 7.7 | 0.6 | 0 | 16.3 | 0.7 | | 44 | | 56 | | | | | | | | |
| 4199.85 | 110 μm | 49 | 66.5 | 0 | 3.7 | 0 | 0 | 29.9 | 0.7 | | 49 | | 51 | | | | | | | | |
| 4199.85 | Vein-fill | 28 | 74.7 | 1.8 | 7.1 | 0 | 0 | 16.4 | 0.9 | 0 | 30 | 0 | 69 | 1.5 | 25 | 75 | 53.8 | 92 | 6 | 2 | 16.3 |
| 4199.85 | Encapsulated | 43 | 57.6 | 0 | 4.2 | 0 | 0 | 38.2 | 1.2 | | 70 | | 30 | | | | | | | | |
| 4509.97 | 110 μm | 32 | 81.9 | 0.3 | 7.9 | 0.6 | 0 | 9.4 | 1.1 | | 59 | | 41 | | | | | | | | |
| 4509.97 | 110 μm | 16 | 78.0 | 1.7 | 13.2 | 0 | 0 | 7.1 | 0.8 | | 12 | | 88 | | | | | | | | |
| 4509.97 | 110 μm | 15 | 71.1 | 0.5 | 16.8 | 0 | 0 | 11.6 | 0.3 | | 44 | | 56 | | | | | | | | |
| 4509.97 | 110 μm | 26 | 79.9 | 0 | 12.6 | 0.8 | 0 | 6.7 | 0.5 | | 20 | | 80 | | | | | | | | |
| 4509.97 | 110 μm | 50 | 84.4 | 0 | 6.7 | 0 | 0 | 8.9 | 2.2 | 0 | 67 | 0 | 33 | | | | | | | | |
| 4509.97 | Vein-fill | 27 | 70.2 | 1.5 | 5.9 | 0 | 0 | 22.4 | 0.4 | 0 | 53 | 0 | 47 | 2.6 | 14 | 86 | | | | | |
| 4509.97 | Encapsulated | 43 | 39.0 | 0 | 4.4 | 0 | 0 | 56.6 | 5.8 | | 3 | | 97 | 0.7 | 15 | 85 | 63.6 | 94 | 5 | 0 | 19.9 |
| 4784.26 | Encapsulated | 48 | 43.3 | 0 | 3.1 | 0 | 0 | 53.6 | 1.4 | | 13 | | 87 | | | | | | | | |
| 4840.15 | Vein-fill | 24 | 76.6 | 1.4 | 5.3 | 0 | 0 | 16.8 | 0.42 | 0 | 66 | 0 | 34 | 0.9 | 16 | 84 | 48.7 | 88 | 12 | 1 | 14.2 |
| 4840.15 | Slot | 18 | 80.3 | 0.2 | 8 | 0 | 0 | 11.6 | 0.4 | 0 | 59 | 0 | 42 | | | | | | | | |
| 4865.09 | Encapsulated | 61 | 42 | 0 | 4.1 | 0 | 0 | 53.9 | 1.5 | | 13 | | 87 | | | | | | | | |
| 4865.09 | 110 μm | 29 | 45.1 | 1.7 | 7.5 | 0 | 0 | 45.7 | 0.7 | | 6 | | 94 | | | | | | | | |
| 4865.09 | 110 μm | 34 | 47.6 | 0.6 | 6.1 | 0 | 0 | 45.7 | 2 | | 9 | | 91 | | | | | | | | |
| 4865.09 | Encapsulated | 45 | 35.3 | 0 | 4.2 | 0 | 0 | 60.6 | 1 | 0 | 12 | 0 | 88 | | | | | | | | |
| 5453.55 | Encapsulated | 62 | 39.5 | 0 | 6.7 | 0 | 0 | 53.7 | 2.3 | | 21 | | 79 | | | | | | | | |
| 5453.55 | Encapsulated | 41 | 45.6 | 0 | 3.7 | 0 | 0 | 50.7 | 1.4 | | 13 | | 87 | | | | | | | | |
| 5463.55 | 110 μm | 33 | 73.9 | 0.1 | 6.6 | 0.5 | 0 | 18.8 | 0.5 | | 56 | | 44 | | | | | | | | |
| 5478.22 | 110 μm | 31 | 65.8 | 0 | 4.4 | 0 | 0 | 29.8 | 0.5 | | 44 | | 56 | | | | | | | | |
| 5478.22 | Vein-fill | 24 | 71.7 | 1.6 | 5.6 | 0 | 0 | 21.1 | 0.38 | 0 | 55 | 0 | 45 | 1.4 | 11 | 89 | 67.2 | 93 | 6 | 1 | 19.6 |
| 5478.22 | Encapsulated | 55 | 47.6 | 0 | 4 | 0 | 0 | 48.4 | 1.5 | 0 | 57 | 0 | 43 | | | | | | | | |

Beta curve merged with Main for *Encapsulated* samples.
Amino and quaternary nitrogen forms = 0 Mole% for all samples.
Samples that report only %aromatic and $\%SO_4$ are curved resolved from the survey scan data. $S^0$, $S = 0$, and $SO_2 = 0$ Mole% for all samples.
Organic oxygen values for small spot and *Encapsulated* samples heavily influenced by inorganic oxygen.

Tables 3a and 3b provide a summary of the percentage of organic carbon, its degree of aromaticity, and the normalized proportion of organic nitrogen, sulfur, and oxygen. Considerable care was taken in data processing for the aromatic carbon of the ground encapsulated samples where the solid bitumen is now mixed with calcite. Small spot and vein-fill samples range typically from 60% to 80% organic carbon. The ground encapsulated samples are considerably lower, with only ~30–50% of the measured carbon reported as organic. The heteroatom values were taken from high-resolution spectra when available. In the absence of high-resolution analysis, a nitrogen value was obtained from the survey analysis and assumed to be all organic. This is a reasonable assumption because nitrogen is revealed to be organic in the high-resolution analyses that were performed. Similarly, sulfur values from the survey scans were used when no high-resolution sulfur analysis was performed. The survey spectra are sufficiently resolved to distinguish inorganic from organic sulfur, but are insufficient to separate the speciation of organic sulfur. Organic oxygen, when not measured by high-resolution analysis, was calculated from the number of C–O bonds in the high-resolution carbon spectra. Assuming that these carbons are associated with C–O–C species (e.g., ethers), the amount of associated oxygen is half that of the measured carbon within this chemical environment. In these cases, it is also assumed that no other oxygen species contribute to the total oxygen content.

## 4. Discussion

### 4.1. Consistency of inorganic elemental composition

As the mineral matrix of the Tengiz core samples is mostly calcite with only minor amounts of anhydrite and clays, simple stoichiometric correlations should exist between the measured amounts of inorganic elements. The consistency of these relationships can serve as a measure of quality control in curve resolution that differentiates inorganic from organic chemical environments.

Calcium is bound mostly as calcite ($CaCO_3$) with minor amounts of anhydrite ($CaSO_4$). Consequently, the number of calcium atoms should be proportional to the sum of the inorganic carbon

Table 3a
T-8 well samples high-resolution/survey organic C, N, S, O

| Depth | Prep/anal. | Per 100 C | $C_{org}$ | Per 100 organic carbon atoms | | | |
|---|---|---|---|---|---|---|---|
| | | $C_{Org}$ | %Aromatic | $N_{org}$ | $S_{org}$ | $O_{org}$ | ΣNSO |
| 3961.8 | Vein-fill | 94.2 | 28 | 0.8 | 0.6 | 3.4 | 4.8 |
| 3961.8 | Slot | 71.5 | 51 | 0.4 | 1.0 | 13.3 | 14.7 |
| 3961.8 | Encapsulated | 66.3 | 49 | 0.9 | 1.4 | 9.7 | 12.0 |
| 3961.8 | Encapsulated | 75.1 | 36 | 0.8 | 1.8 | 8.6 | 11.2 |
| 3972 | Vein-fill | 88.1 | 26 | 1.0 | 1.5 | 7.3 | 9.8 |
| 3972 | Slot | 92.8 | 51 | 0.8 | 0.3 | 6.9 | 8.0 |
| 3972 | Encapsulated | 71.8 | 20 | 1.1 | 1.9 | 8.7 | 11.7 |
| 3977 | Vein-fill | 85.7 | 68 | 1.5 | 2.8 | 7.8 | 12.1 |
| 3977 | Slot | 78.3 | 42 | 1.2 | 1.5 | 6.5 | 9.2 |
| 3983.5 | Slot | 83.3 | 43 | 3.8 | 1.0 | 11.6 | 16.4 |
| 3983.5 | Slot | 77.3 | 26 | 0.7 | 1.4 | 8.8 | 10.9 |
| 3983.5 | Encapsulated | 69.7 | 21 | 0.6 | 1.8 | 8.1 | 10.5 |
| 4016.5 | Slot | 97.9 | 56 | 1.3 | 0.1 | 16.4 | 17.8 |
| 4016.5 | Encapsulated | 60.7 | 65 | 0.4 | 1.1 | 11.5 | 13.0 |
| 4044.5 | Slot | 98.8 | 61 | 0.6 | 0.1 | 19.2 | 19.9 |
| 4044.5 | Slot | 97.4 | 72 | 0.3 | 0.6 | 11.3 | 12.2 |
| 4044.5 | Encapsulated | 64.4 | 46 | 0.5 | 1.5 | 10.2 | 12.2 |
| 4056.5 | Encapsulated | 72.8 | 45 | 0.7 | 1.7 | 8.4 | 10.8 |
| 4056.5 | Slot | 90.6 | 30 | 1.4 | 1.1 | 12.4 | 14.9 |
| 4123 | Slot | 81.0 | 59 | 1.9 | 0.9 | 7.9 | 10.7 |
| 4123 | Encapsulated | 71.5 | 58 | 0.8 | 1.6 | 11.3 | 13.7 |
| 4137 | Slot | 76.9 | 63 | 1.3 | 1.3 | 13.5 | 16.1 |
| 4157.77 | Slot | 92.4 | 58 | 1.4 | 1.0 | 8.4 | 10.8 |
| 4186 | Vein-fill | 88.1 | 44 | 0.4 | 0.9 | 5.9 | 7.2 |
| 4186 | Slot | 81.8 | 49 | 0.7 | 1.1 | 11.2 | 13.0 |
| 4328 | Vein-fill | 93.8 | 54 | 0.3 | 0.5 | 3.2 | 4.0 |
| 4328 | Slot | 86.0 | 54 | 0.4 | 0.5 | 3.7 | 4.6 |

Table 3b
T-5056 well samples high-resolution/survey organic C, N, S, O (O calculated from C–O when not available by direct measurement)

| Depth | Prep/anal. | Per 100 C | $C_{org}$ | Per 100 organic carbon atoms | | | |
|---|---|---|---|---|---|---|---|
| | | $C_{org}$ | %Aromatic | $N_{org}$ | $S_{org}$ | $O_{org}$ | ΣNSO |
| 3913.26 | Vein-fill | 88.8 | 14 | 1.5 | 1.5 | 7.4 | 10.4 |
| 3913.26 | Slot | 69.9 | 45 | 2.2 | 0.8 | 3.3 | 6.3 |
| 3957.77 | 110 μm | 81.9 | 35 | 1.8 | 1.1 | 3.1 | 6.0 |
| 3957.77 | Slot | 86.3 | 15 | 2.5 | 1.9 | 7.3 | 11.7 |
| 3995.08 | 110 μm | 91.1 | 18 | 0.7 | 0.8 | 5.2 | 6.7 |
| 3995.08 | 110 μm | 94.6 | 52 | 1.6 | 1.2 | 11.9 | 14.7 |
| 3995.08 | 110 μm | 93.0 | 21 | 1.0 | 0.8 | 7.5 | 9.3 |
| 3995.08 | Vein-fill | 82.8 | 24 | 1.5 | 1.7 | 10.8 | 14.0 |
| 3995.43 | 110 μm | 87.7 | 45 | 2.2 | 0.8 | 14.3 | 17.3 |
| 3995.43 | Vein-fill | 74.2 | 63 | 0.2 | 0.6 | 3.8 | 4.6 |
| 3995.43 | Slot | 78.7 | 38 | 3.3 | 0.4 | 4.8 | 8.5 |
| 4190.22 | Slot | 81.4 | 27 | 1.0 | 0.7 | 14.0 | 15.7 |
| 4199.85 | Encapsulated | 52.3 | 25 | 1.3 | 1.3 | 7.6 | 10.2 |
| 4199.85 | 110 μm | 86.0 | 49 | 1.7 | 1.9 | 5.2 | 8.9 |
| 4199.85 | 110 μm | 84.5 | 32 | 0.8 | 0.5 | 10.8 | 12.1 |
| 4199.85 | 110 μm | 83.7 | 16 | 2.1 | 0.7 | 5.2 | 8.0 |
| 4199.85 | 110 μm | 70.1 | 15 | 0.7 | 0.7 | 2.8 | 4.2 |
| 4199.85 | Vein-fill | 83.6 | 26 | 0.9 | 0.9 | 4.8 | 6.6 |
| 4199.85 | Encapsulated | 61.8 | 50 | 0.5 | 1.2 | 3.8 | 5.5 |
| 4509.97 | 110 μm | 90.6 | 29 | 1.8 | 1.1 | 4.8 | 7.7 |
| 4509.97 | 110 μm | 92.9 | 34 | 1.2 | 0.8 | 8.5 | 10.5 |
| 4509.97 | 110 μm | 88.4 | 33 | 0.4 | 0.3 | 11.8 | 12.5 |
| 4509.97 | 110 μm | 93.3 | 31 | 1.3 | 0.5 | 7.9 | 9.7 |
| 4509.97 | 110 μm | 91.1 | 17 | 2.6 | 1.5 | 4.0 | 8.1 |
| 4509.97 | Vein-fill | 77.6 | 62 | 0.7 | 0.2 | 3.7 | 4.6 |
| 4509.97 | Encapsulated | 55.1 | 28 | 0.5 | 1.8 | 3.6 | 5.9 |
| 4784.26 | Encapsulated | 46.4 | 27 | 0.9 | 1.4 | 3.7 | 6.0 |
| 4840.15 | Vein-fill | 83.2 | 24 | 0.9 | 0.3 | 5.9 | 7.1 |
| 4840.15 | Slot | 88.4 | 24 | 0.3 | 0.3 | 5.0 | 5.6 |
| 4865.09 | Encapsulated | 46.1 | 40 | 0.3 | 1.5 | 4.9 | 6.7 |
| 4865.09 | 110 μm | 54.3 | 43 | 0.4 | 0.7 | 8.3 | 9.4 |
| 4865.09 | 110 μm | 54.3 | 43 | 0.3 | 2.0 | 6.4 | 8.7 |
| 4865.09 | Encapsulated | 39.4 | 41 | 0.1 | 1.0 | 6.2 | 7.3 |
| 5453.55 | Encapsulated | 46.3 | 48 | 0.3 | 2.3 | 8.5 | 11.1 |
| 5453.55 | Encapsulated | 49.3 | 61 | 0.6 | 1.4 | 4.1 | 6.1 |
| 5463.55 | 110 μm | 81.2 | 45 | 0.7 | 0.5 | 4.5 | 5.7 |
| 5478.22 | 110 μm | 70.2 | 62 | 1.0 | 0.5 | 3.3 | 4.8 |
| 5478.22 | Vein-fill | 78.9 | 41 | 1.2 | 0.4 | 3.9 | 5.5 |
| 5478.22 | Encapsulated | 51.6 | 55 | 0.3 | 0.8 | 4.3 | 5.4 |

All values for $C_{org}$ and % aromaticity are from high-resolution carbon analyses.
Survey scan values are reported where $N_{org}$ and $S_{org}$ values are not available from high-resolution analysis.
$O_{org}$ calculated from the carbon high-resolution analysis where $O_{org}$ values are not available from high-resolution analysis. This calculation, $100 \times (1/2 \cdot C - O/C_{org})$, assumes that all organic oxygen is bound as ether linkages.

and sulfur atoms as illustrated in Fig. 4. Samples from T-5056 correspond well to the unity trend line. Calcium is enriched above carbon parity line in samples from the T-8 well with Ca values above ~25%, suggesting that other trace minerals may contribute to the calcium response. The correlation between calcium and inorganic oxygen yields a stoichiometric relationship of 3.2 (Fig. 5). This is slightly higher than expected for pure calcite, and may be attributed to the presence of anhydrite.

### 4.2. Aromaticity and NSO content of solid bitumens

Tengiz solid bitumens exhibit a broad distribution of aromaticity and heteroatom content. The aromatic carbon content is particularly anomalous (Fig. 6) ranging from 14% to 72%. In contrast, petroleum asphaltenes, precipitated from a suite of oils derived from a variety of common source facies, range from ~35% to 50% aromatic carbon. When pyrolyzed, asphaltene residues exceed 80% aroma-

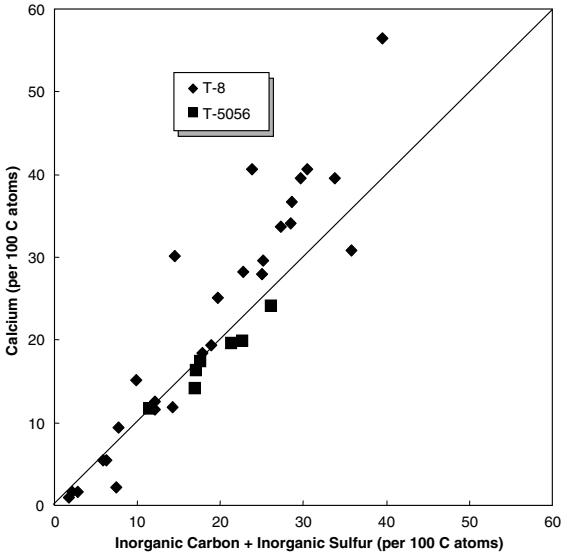


Fig. 4. Relationship between the number of calcium atoms and the sum of inorganic carbon and inorganic sulfur atoms per 100 carbon atoms in Tengiz solid bitumen samples. Samples from the T-5056 well are consistent with the unity trend line. Calcium is slightly enriched in samples from the T-8 above ~25% Ca, suggesting that other trace minerals may contribute to the calcium response. All samples prepared as vein-fill concentrates or as encapsulated powders.

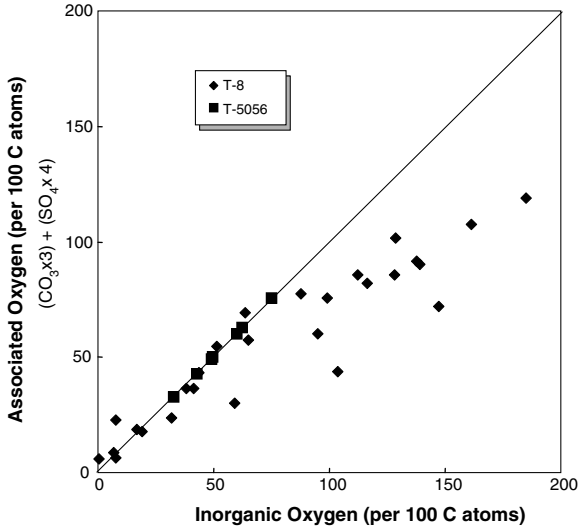


Fig. 5. Relationship between the number of calcium atoms and inorganic oxygen atoms per 100 carbon atoms in Tengiz solid bitumen samples. The data fits best with a Ca to O distribution of 1:3.2, which is slightly higher than the stoichiometric 1:3 ratio of calcite. All samples prepared as vein-fill concentrates or as encapsulated powders.

ticity, indicating that thermally altered asphaltenes may have more than >50% aromatic carbon. Given these limits, only a fraction of the Tengiz solid bitumens are consistent with asphaltene precipitates or their thermally stressed equivalents, as approximately 40% of the samples contain less than 35% aromatic carbon. The lowest values are associated mostly with the small spot samples.

The abundance of organic nitrogen in the Tengiz solid bitumens (0–3.3 atoms *N*/100 atoms carbon) is similar to that of petroleum asphaltenes and their thermally stressed equivalents (typically, ~0–4

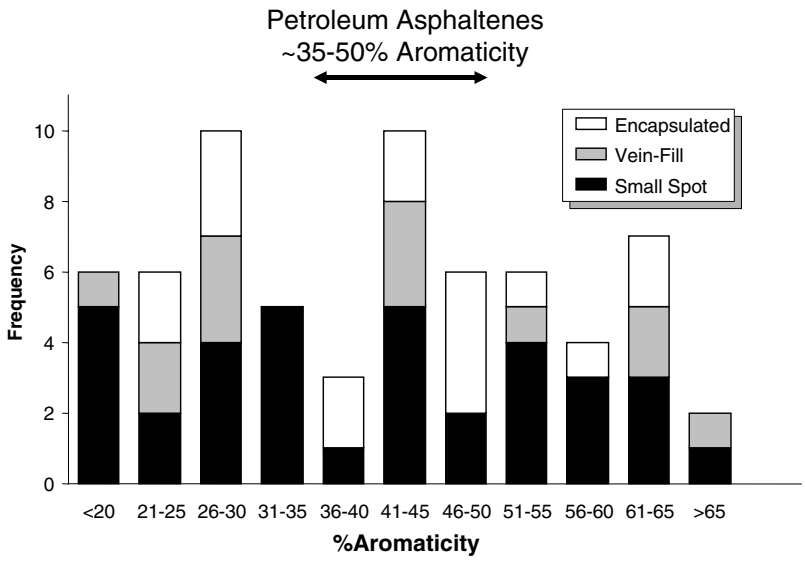


Fig. 6. Distribution of %aromaticity of organic carbon in Tengiz solid bitumens sorted by sample type. The range of aromaticity of petroleum asphaltenes (~35–55%) from a variety of common source kerogens is shown for reference.

atoms $N$/100 atoms carbon). The organic nitrogen in Tengiz solid bitumens is present only as pyrrolic and pyridinic species in a proportion similar to the distribution observed in asphaltenes, which ranges from ~65% to 80% pyrrolic nitrogen.

Encapsulated bitumens appear to be preferentially enriched in organic sulfur relative to small spot analyses (Fig. 7). Moreover, Tengiz solid bitumens essentially contain only aromatic (thiophenic) sulfur that normally is characteristic of a high state of maturation. This compositional difference most likely reflects the chemistry of the precursor compounds, as thermal stress does not significantly influence the overall sulfur content of asphaltene residues. Petroleum asphaltenes typically contain 50–80% aromatic sulfur, the balance being non-aromatic species such as alkylsulfides. Upon thermal alteration, non-aromatic sulfur is lost completely at a state corresponding to carbon aromaticity >80%, a condition not observed in the Tengiz solid bitumens. The absence of non-aromatic sulfur forms at relatively low aromaticity is a distinctive feature of these reservoir solids.

Many Tengiz solid bitumens have unusually high concentrations of organic oxygen compared to petroleum asphaltenes (Fig. 8). Petroleum asphaltenes rarely range above 6 atoms organic oxygen/

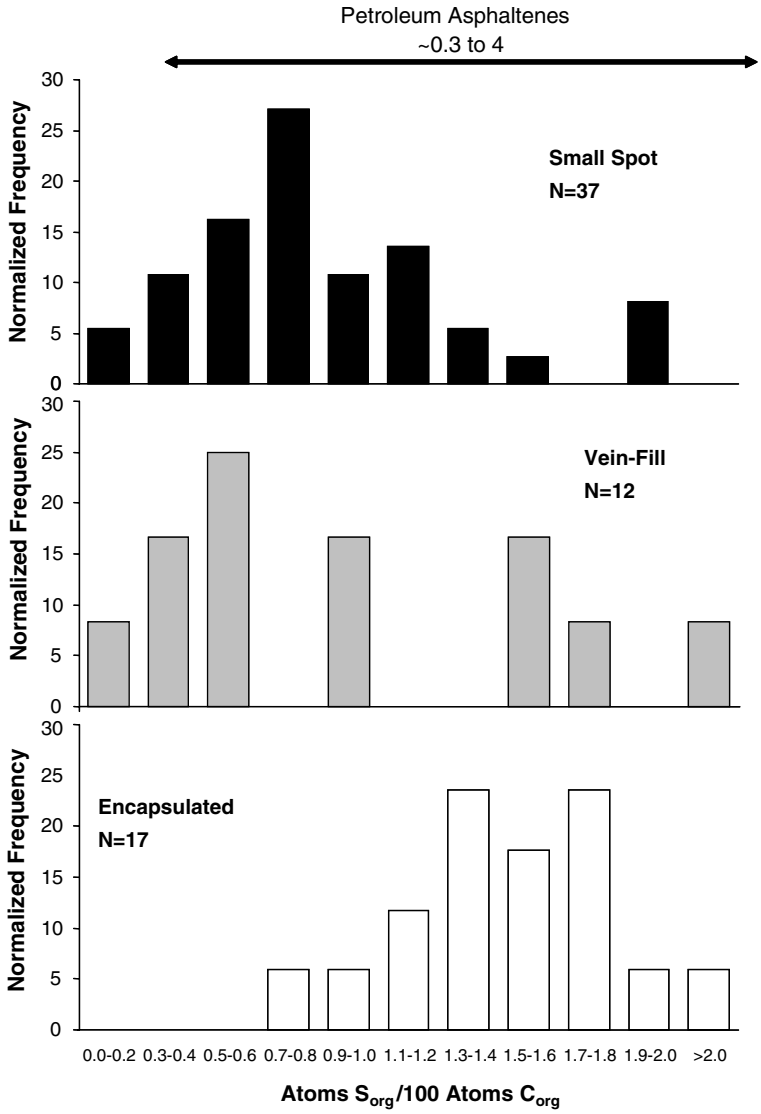


Fig. 7. Distribution of the number of organic sulfur atoms per 100 atoms of organic carbon in Tengiz solid bitumens sorted by sample type. The range observed for petroleum asphaltenes from a variety of common source kerogens is shown for reference.

100 atoms carbon with the ratio remaining roughly constant upon pyrolysis. While a portion of solid bitumens exhibit values similar to asphaltenes, many are highly enriched in organic oxygen. The highest values are associated with the small spot analysis. Most of this organic oxygen appears in an ether environment, with only trace or minor amounts in carbonyl or carboxyl forms.

### 4.3. Depth–stratigraphic relationships

There are no discernable trends in the chemical composition of the Tengiz solid bitumens with depth or stratigraphy. One might expect the aromaticity of the solid bitumens to increase with depth and increasing thermal stress. This effect is not observed (Fig. 9). Similarly, the relative abundance and speciation of the heteroatoms is independent of depth or stratigraphy.

Depth trends in Tengiz solid bitumen reflectance have been reported and used to constrain paleotemperature models (Baskin et al., 1997; Hallager et al., 1997; Hwang et al., 1998; Schoellkopf and Hallager, 1998). We see no corresponding trends in the chemistry of the solid bitumens; however, the encapsulated samples tend to be more aromatic than vein-fill samples from the same depth. Since bitumen reflectance is controlled mostly by the degree of aromatization, vein-fill bitumens, which are observed to be most abundant in the shallowest strata, should exhibit lower reflectance than encapsulated, micropore bitumens, which are predomi-

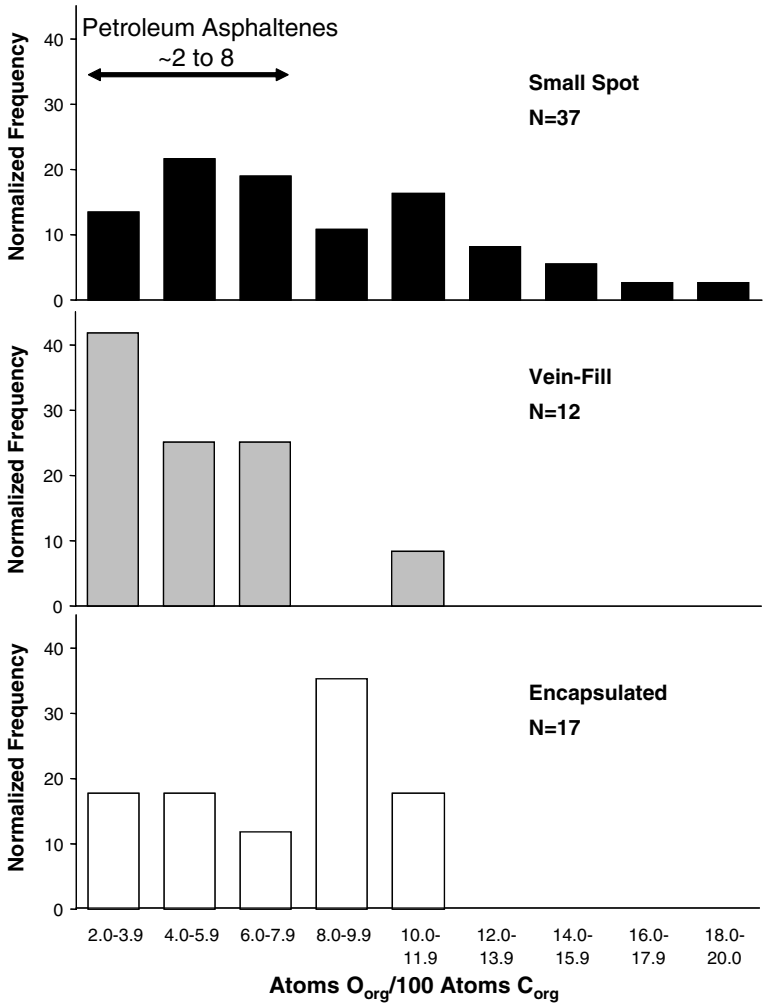


Fig. 8. Distribution of the number of organic oxygen atoms per 100 atoms of organic carbon in Tengiz solid bitumens sorted by sample type. The range observed for petroleum asphaltenes from a variety of common source kerogens is shown for reference.

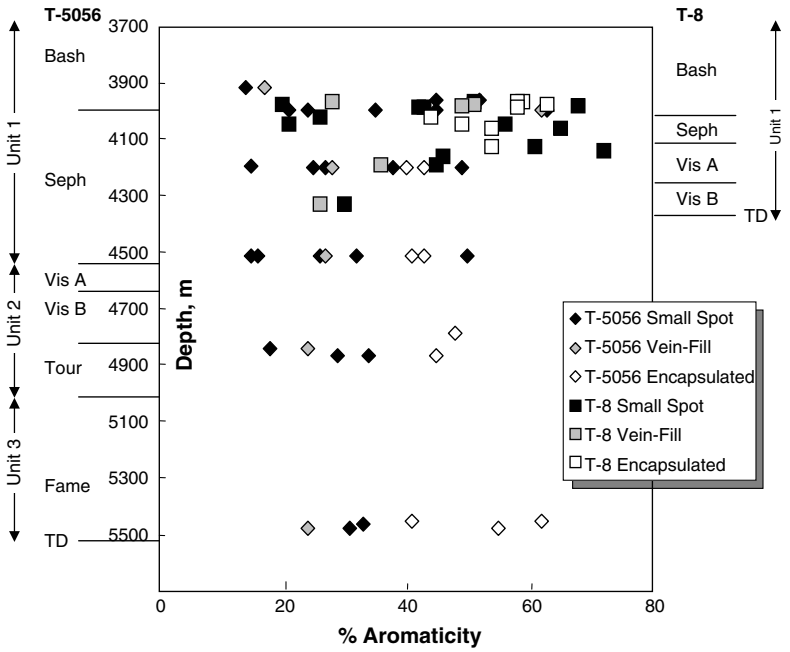


Fig. 9. Plot of percentage aromatic carbon in Tengiz solid bitumens versus sample depth (with stratigraphy).

nant in the lower strata. We believe reported increases in solid bitumen reflectance with depth do not reflect increasing thermal alteration, but are an artifact of the relative abundance of bitumens having different chemical origins.

### 4.4. Reactive polar precipitation

XPS analysis shows that all Tengiz solid bitumens are enriched in ether-linked oxygen atoms relative to asphaltene precipitates or their pyrolyzate residues and that organic sulfur occurs only in an aromatic (thiophenic) state. The degree of aromatization varies and two different, chemically distinct phases can be distinguished (Fig. 10). One phase, predominant in the micropores, has a composition similar to petroleum asphaltene precipitates that have been thermally and/or chemically altered. The other phase, found mostly in vein-fills and fractures, has a much lower degree of aromaticity than petroleum asphaltenes. This hydrogen-rich material appears to be preferentially formed on exterior surfaces and is best characterized by several small spot analyses with low aromaticity and a high ratio of C–O species.

We propose that the composition of these hydrogen-rich organic films can be explained by the reaction of low-molecular weight polar compounds, forming a naphthenic-rich solid bitumen. Petroleum asphaltenes and NSO polar compounds have different solubilities. Asphaltenes precipitate through the addition of light hydrocarbons or a decrease in reservoir pressure, while polar compounds remain in solution. The solubility differences are attributed to variations in molecular weight, aromaticity, and polar functionality. Asphaltenes range from ~500 to 1000 Da, while polars range from ~250 to 600 Da (Groenzin and Mullins, 2000; Qian et al., 2001). Polar compounds tend to be more saturated than asphaltic compounds. The chemical environments of the NSO atoms within the polar and asphaltic compounds are believed to be similar.

A hydrogen-rich precipitate could arise if polar compounds react and condense, forming a product that is no longer soluble in the reservoir petroleum fluid – a process we term "reactive polar precipitation". A likely mechanism for this reaction is the thermal cracking of labile sulfur species (e.g., mercaptans, thialanes, and disulfides) producing reactive free radicals and $H_2S$. Such reactions can take place under typical reservoir temperatures ($\gtrsim 100$ °C). The radicals then react with hydroxyl groups to form stable ether linkages (Fig. 11). The condensed polar compounds can then precipitate because the reacted product is no longer compatible with hydrocarbon-rich oil.

Similar reactions can account for conversion of precipitated polars and asphaltenes to solid bitumens that are insoluble in laboratory solvents.

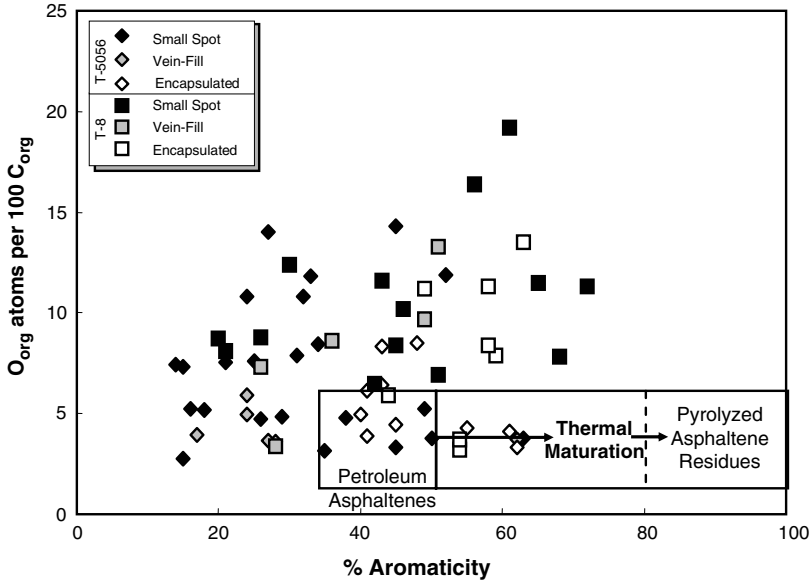


Fig. 10. Aromatic carbon versus number of organic oxygen atoms per 100 atoms of organic carbon. Many Tengiz solid bitumens are less aromatic and exhibit enriched ether oxygen values compared to petroleum asphaltenes and their thermally altered equivalents.

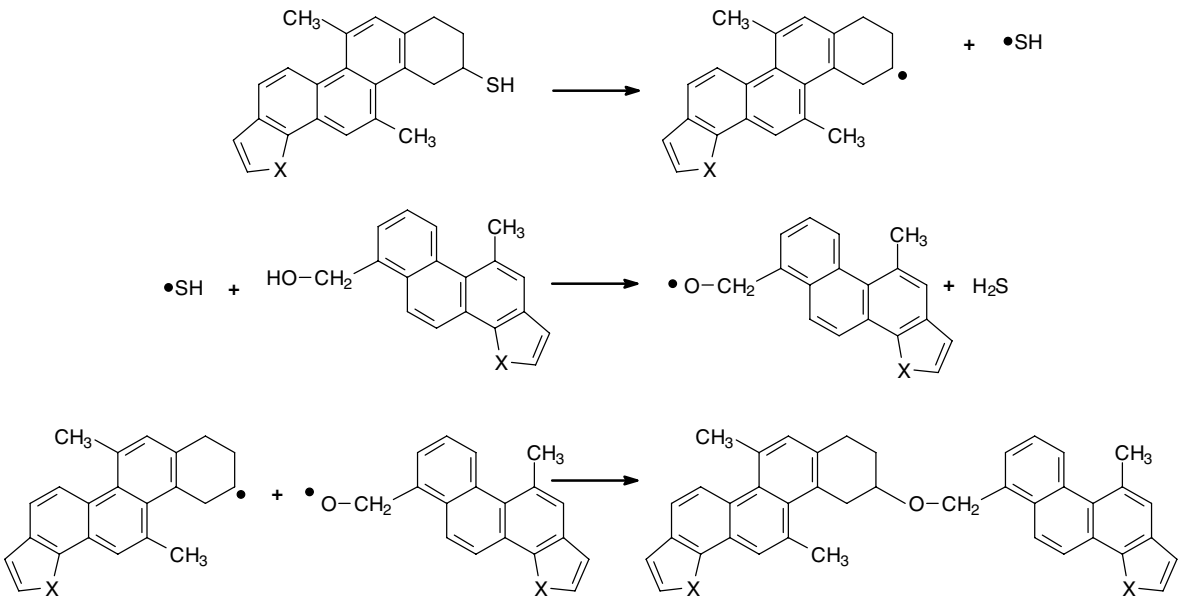


Fig. 11. Proposed reaction scheme for the generation of polar precipitates. X = N, S, or O.

One additional ether cross-linkage between precipitated asphaltene or reacted polar molecules is sufficient to alter the solubility of the condensed molecule such that it is no longer soluble in toluene. This reaction mechanism accounts for (1) enrichments in ether-linked oxygen and aromatic sulfur, (2) the absence of non-aromatic sulfur, and (3) the relatively unaltered nature of nitrogen that is observed in the Tengiz solid bitumens. It also provides a mechanism to form solid bitumens at the relatively low temperatures that the reservoir rocks experienced.

## 5. Solid bitumen formation in Tengiz Field

The hypothesis for reactive polar precipitation and solid bitumen formation via ether-linkage reactions agrees well with current models for the

geohistory of Tengiz Field. The reservoir was charged initially during the early Triassic Period with an asphaltene-bearing oil. Upon seal failures (between 220 and 125 Ma), asphaltenes dropped out of solution due to depressurization. This early asphaltic precipitate, present in both micro- and macro-pores, experienced low reservoir temperatures for as long as 250 million years, resulting in partial aromatization and ether-linkage reactions that produced hydrogen-poor, oxygen-rich solid bitumen. The coincidence of reservoir depressurization and peak oil and gas generation from Paleozoic source rocks during the Late Jurassic–Early Cretaceous resulted in precipitation of large volumes of asphaltenes along migration pathways (flanks and rim features) mainly in fractures and other permeable pathways open to flow. Following re-establishment of a seal and refilling of the reservoir with oil, reactive polar compounds precipitated from the reservoir hydrocarbons producing an aliphatic-rich coating on previously precipitated asphaltene. Such surface coatings would be most abundant in vein-fill samples because asphaltenes precipitated in the micropore spaces either were completely sealed or had restricted access to the polar compounds during the second hydrocarbon charge. Once precipitated, the polar and asphaltic materials would further condense to their present solid, toluene-insoluble state.

When characterized as a large homogenized sample, such as obtained after acid digestion of several grams of reservoir rock, Tengiz solid bitumens exhibit little chemical variation. However, significant chemical and optical variabilities are observed on a microscopic scale. Chemically, individual Tengiz bitumens vary greatly in their solubility by strong polar solvents and in the distribution of hydrocarbon products using micro-laser pyrolysis. Optically, multiple populations of bitumen with different morphology and reflectance (~0.2–1.5%) exist within the same rock sample (Hwang et al., 1998; Warner et al., 1999). Optical heterogeneity exists within individual bitumen particles that have distinct rimming features of low reflecting material surrounding a higher reflecting bitumen mass (L.D. Stasiuk, pers. comm.). High reflectivity measurements of some solid bitumens but not others lead to the hypothesis that hot hydrothermal fluids invaded the Tengiz reservoir from deeper in the basin prior to the final filling of the reservoir (Hallager et al., 1997; Warner et al., 1999).

Our model, where the bulk of Tengiz solid bitumen is chemically altered asphaltenes with variable surface coatings of precipitated polar compounds, offers an alternative explanation for these anomalous observations. Asphaltenes that precipitated during early episodes of seal breach have undergone a substantial degree of thermal conversion under prolonged exposure to normal reservoir temperatures (Pottorf et al., 2003). Moderate temperatures of thermal conversion (<120 °C) are consistent with fluid inclusion homogenization temperatures (Warner et al., 1999; Tseng and Pottorf, 2003) and XPS measurements of Tengiz solid bitumen %aromaticity (≤72%), which are consistently below values observed for asphaltene pyrolyzates (>80%). It is possible that such reactions produce aromatic-rich residues, that when combined with the ether cross-linkage reactions, could result in high reflectivity. Unanswered is whether such reactions can result in mosaic textures that imply rapid heating by hot hydrothermal fluids. Polar precipitation readily accounts for the distinct rimming features of low reflective material coating more reflective inner cores. The chemical precipitation of this material will post-date the precipitation of asphaltenes and coat aromatic-rich, high reflective solid bitumen with naphthenic-rich, low reflective organic films. Hence, the co-occurrence of thermally altered precipitated asphaltenes and low-reflectivity polar precipitates can explain the wide variations in reflectivity that may occur within a single sample, and differences in dissolution in laboratory solvents. Additionally, polar precipitation explains the very low content of polars in produced Tengiz oil (~3% of the $C_{15+}$ fraction) and provides a mechanism to explain the occurrence of solid bitumens at different stages of the paragenetic sequence.

## 6. Global occurrence of reactive polar precipitates

The polar precipitation model discovered in cores from Tengiz Field is applicable to other structures within the North Caspian basin, such as Korolev and Kashagnan that contain varying amounts of solid bitumen. There is every reason to believe that the process is a common occurrence in petroleum systems where reservoirs have been exposed to sufficient temperatures to promote free radical formation from labile, non-aromatic sulfur species. One such documented occurrence may be solid bitumens reported in Triassic carbonate rocks of the Shiwan Dashan Basin, South China (Gao et al., 2001). This

stratum experienced similar burial depths and temperatures (~4300 m depth, 110 °C) and solid bitumens from the Shiwan Dashan Basin exhibit similar unusual optical and chemical properties as Tengiz. Gao et al. (2001) attributed formation of this material to a pressure effect, terming the material "compressively matured bitumen", but it is unclear how pressure alone could promote the conversion of associated oil to solid bitumen.

The generation of polar precipitates that are sufficiently thick to be readily seen might require specific conditions, such as stable hydrocarbon-filled reservoirs maintaining relatively mild temperatures for >100 million years. Under less optimal conditions, polar precipitation might still occur, but produce only very thin surface coatings that are undetectable by conventional optical microscopy. Such coatings could have significant impact on reservoir properties, such as surface wetability and precipitation of late diagenetic cements.

## 7. Conclusions

X-ray photoelectron spectroscopy of solid bitumens from Tengiz Field reveals that the bitumens consist mainly of chemically altered asphaltenes coated with varying amounts of a hydrogen-rich polar material. We hypothesize that this material results from a newly described reservoir process we term reactive polar precipitation. A likely pathway for the formation of aliphatic- and oxygen-rich solid bitumen coating under low, reservoir temperatures (<120 °C) is the production of free radicals from the thermal cleavage of labile, non-aromatic sulfur species that then react with hydroxyl groups to form ether-linked products. The ether cross-linkage reactions also account for the transformation of the precipitated reactive polars and asphaltenes into solid bitumens that are insoluble in toluene and more polar laboratory solvents. Reactive polar precipitation offers an explanation for many of the unusual optical and chemical properties reported for the solid bitumens from the North Caspian Basin and is consistent with the observed paragenetic sequence and with current geohistory models at Tengiz.

## Acknowledgments

We thank Rick Haack, Bill Hallager, and Ken Peters for their insightful reviews and suggestions for improvements to this paper. We also thank the managements of ExxonMobil Development, Upstream Research, and Research & Engineering companies for supporting this work and TengizChevroil and its shareholder companies (ChevronTexaco, ExxonMobil, Kazmunaigaz, and BPLukArco) for permission to publish this paper.

*Associate Editor*—**Kenneth Peters**

## References

Anissimov, L., Postnova, E., Merkulov, O., 2000. Tengiz oilfield: geological model based on hydrodynamic data. Petroleum Geoscience 6, 59–65.

Baskin, D.K., Garber, R.A., Harris, P.M., Warner, J.L., Hallager, W.S., Kubentay, S., 1997. Two-stage hydrocarbon migration model for the Tengiz Field, Kazakstan. AAPG Annual Convention, Abstracts. Dallas, Texas, April 6–9, Abstracts, p. 9.

Curiale, J.A., 1986. Origin of solid bitumens, with emphasis on biological marker results. Organic Geochemistry 10, 559–580.

Effimoff, I., 2001. Future hydrocarbon potential of Kazakhstan. In: Downey, M.W., Threet, J.C., Morgan, W.A. (Eds.), Petroleum Provinces of the Twenty-first Century, vol. 74. AAPG Memoir, pp. 243–258.

Gao, Z.-N., Chen, Y.-Y., Niu, F., 2001. Compressively matured solid bitumen and its geochemical significance. Geochemical Journal 35, 155–168.

Groenzin, H., Mullins, O.C., 2000. Molecular size and structure of asphaltenes from various sources. Energy & Fuels 14, 677–684.

Hallager, W.S., Suisinov, K., Baskin, D.K., Garber, R.A., Harris, P.M., Warner, J.L., 1997. Two-stage hydrocarbon migration model for the Tengiz Field, Kazakhstan. American Association of Petroleum Geologists Bulletin 81, 1380.

Harris, P.M., Warner, J.L., 2001. Slope deposits of the Tengiz platform; core and log data from a key well. AAPG Annual Meeting, Denver, Colorado, June 3–6, Abstracts, pp. 64–65.

Harris, P.M., Garber, R.A., Clark, M.E., 2000. Geologic framework for the Tengiz and Korolev isolated carbonate platforms, Kazakhstan. American Association of Petroleum Geologists Bulletin 83, 225–229.

Harris, P.M., Garber, R.A., Warner, J.L., 2001. Characterizing Tengiz platform deposits; core and log data from a key well. AAPG Annual Meeting, Denver, Colorado, June 3–6, Abstracts, pp. 80–81.

Hwang, R.J., Teerman, S.C., Carlson, R.M., 1998. Geochemical comparison of reservoir solid bitumens with diverse origins. Organic Geochemistry 29, 505–517.

James, W.L., Francis, B.P., Harris, P.M., Clark, M., 2003. Stratigraphy, lithofacies, and reservoir distribution, Tengiz Field, Kazakhstan. In: Ahr, W.M., Harris, P.M., Morgan, W.A., Somerville, I.D. (Eds.), Permo-Carboniferous Carbonate Platforms and Reefs, vol. 78. Society for Sedimentary Geology Special Publication, pp. 351–394.

Karpov, P.A., Vachugova, L.I., Tymochko, T.G., Khomutnikov, R.P., Iurkiv, N.I., Karpov, V.P., 1985. Solid bitumens of productive limestones of the Tengiz oil pool. Doklady Akademii Nauk USSR 284, 937–939 (in Russian).

Kelemen, S.R., Kwiatek, P.J., 1995. Quantification of organic oxygen species on the surface of fresh and reacted Argonne premium coal. Energy & Fuels 9, 841–848.

Kelemen, S.R., George, G.N., Gorbaty, M.L., 1990. Direct determination and quantification of sulphur forms in heavy petroleum and coals: 1. The X-ray photoelectron spectroscopy (XPS) approach. Fuel 69, 939–944.

Kelemen, S.R., Rose, K.D., Kwiatek, P.J., 1993. Carbon aromaticity based on XPS-Π to Π* signal intensity. Applied Surface Science 64, 167–173.

Kelemen, S.R., Gorbaty, M.L., Kwiatek, P.J., 1994. Quantification of nitrogen forms in Argonne premium coals. Energy & Fuels 8, 896–906.

Kelemen, S.R., Freund, H., Gorbaty, M.L., Kwiatek, P.J., 1999. Thermal chemistry of nitrogen in kerogen and low-rank coal. Energy & Fuels 13, 529–538.

Kelemen, S.R., Afeworki, M., Gorbaty, M.L., Kwiatek, P.J., Solum, M.S., Hu, J.Z., Pugmire, R.J., 2002. XPS and $^{15}N$ NMR study of nitrogen forms in carbonaceous solids. Energy & Fuels 16, 1507–1515.

Lisovsky, N.N., Gogonenkov, G.N., Petzoukha, Y.A., 1992. The Tengiz oil field in the pre-Caspian Basin of Kazakhstan (former USSR); supergiant of the 1980s. In: Halbouty, M.T. (Ed.), Giant Oil and Gas Fields of the Decade 1978–1988, vol. 54. AAPG Memoir, pp. 101–122.

Lomando, A.J., 1992. The influence of solid reservoir bitumen on reservoir quality. American Association of Petroleum Geologists Bulletin 76, 1137–1152.

Patel, P.D., Christman, P.G., Gardner, J.W., 1987. Investigation of unexpectedly low field-observed fluid mobilities during some $CO_2$ tertiary floods. SPE Reservoir Engineering, Paper No. 14308, pp. 507–513.

Peters, K.E., Walters, C.C., Moldowan, J.M., 2004. The Biomarker Guide Biomarkers and Isotopes in Petroleum Exploration and Earth History, vols. 1 and 2. Cambridge University Press, New York, NY.

Pottorf, R.J., Tseng, H.-Y., Hicks, P., Putney, K., Curry, D., Mankiewicz, P., Gray, G., 2003. Timing, distribution and origin of bitumen formation at Tengiz Field, Kazakhstan. In: Cubbitt, J., England, W., Larter, S., Macleod, G. (Eds.), Conference Abstracts: Geochemistry of Reservoirs II – Linking Reservoir Engineering & Geochemical Models, February 3–4. Geological Society London, Burlington House.

Qian, K., Rodgers, R.P., Hendrickson, C.L., Emmett, M.R., Marshall, A.G., 2001. Reading chemical fine print: resolution and identification of 3000 nitrogen-containing aromatic compounds from a single electrospray ionization Fourier Transform ion cyclotron resonance mass spectrum of heavy petroleum crude oil. Energy & Fuels 15, 492–498.

Rogers, M.A., McAlary, J.D., Bailey, N.J.L., 1974. Significance of reservoir bitumens to thermal-maturation studies, Western Canada Basin. American Association of Petroleum Geologists Bulletin 58, 1806–1824.

Schoellkopf, N.B., Hallager, W.S., 1998. Burial history and charge model, Tengiz Field, Kazakhstan. AAPG Annual Meeting, Salt Lake City, Utah, May 17–20, Abstract.

Tseng, H.Y., Pottorf, R.J., 2003. The application of fluid inclusion PVT analysis to studies of petroleum migration and reservoirs. Journal of Geochemical Exploration 78–79, 433–436.

Tverdova, R.A., Volkova, T.P., Skibitskaya, N.A., 1991. Characteristics of solid bitumens of sub-salt sedimentary rocks of Tengiz Field. Petroleum Geology 25, 285.

Warner, J.L., Baskin, D.K., Hwang, R.J., Clark, M.E., 1999. Geochemical evidence for two stages of hydrocarbon generation in Tengiz and the origin of solid bitumen. Annual AAPG-SEPM Convention, (San Antonio, April 11–14), Book of Abstracts, pp. A145–A146.

Weber, L.J., Francis, B.P., Harris, P.M.H., Clark, M., 2004. Sequence stratigraphy and reservoir prediction of the giant Tengiz Field, Kazakhstan. Bulletin of the Houston Geological Society 46, 19–21.